

# UniCom: Unified Multimodal Modeling via Compressed Continuous Semantic Representations

Yaqi Zhao<sup>1,3\*</sup>, Wang Lin<sup>2,3\*</sup>, Zijian Zhang<sup>3</sup>, Miles Yang<sup>3</sup>,  
Jingyuan Chen<sup>2,†</sup>, Wentao Zhang<sup>1,†</sup>, Zhao Zhong<sup>3</sup>, Liefeng Bo<sup>3</sup>  
<sup>1</sup>Peking University <sup>2</sup>Zhejiang University <sup>3</sup>Tencent Hunyuan

Project Page: <https://miazhao7708.github.io/UniComPage/>

## Abstract

Current unified multimodal models typically rely on discrete visual tokenizers to bridge the modality gap. However, discretization inevitably discards fine-grained semantic information, leading to suboptimal performance in visual understanding tasks. Conversely, directly modeling continuous semantic representations (e.g., CLIP, SigLIP) poses significant challenges in high-dimensional generative modeling, resulting in slow convergence and training instability. To resolve this dilemma, we introduce UniCom, a unified framework that harmonizes multimodal understanding and generation via compressed continuous representation. We empirically demonstrate that reducing channel dimension is significantly more effective than spatial downsampling for both reconstruction and generation. Accordingly, we design an attention-based semantic compressor to distill dense features into a compact unified representation. Furthermore, we validate that the transfusion architecture surpasses query-based designs in convergence and consistency. Experiments demonstrate that UniCom achieves state-of-the-art generation performance among unified models. Notably, by preserving rich semantic priors, it delivers exceptional controllability in image editing and maintains image consistency even without relying on VAE.

## 1 Introduction

The pursuit of unified multimodal models Pan et al. (2025a); Deng et al. (2025); Tong et al. (2026), capable of both understanding and generating content across modalities such as text and images, represents a significant paradigm shift in artificial intelligence. A key insight from this evolution is that unification is not merely an engineering challenge of connecting modules. It fundamentally questions the representational divide between discrete, symbolic reasoning (language) and continuous, perceptual synthesis (vision). The ongoing research is, in essence, searching for a “unified token”—a common representational substrate that can seamlessly flow between understanding and generation, between text and pixels, while being efficiently processed by a scalable neural architecture.

Achieving such unification critically depends on how visual information is represented, making the design of visual encoders a central challenge. Some compromise approaches Chen et al. (2025e); Wang et al. (2025); Qu et al. (2025); Xie et al. (2025b); Deng et al. (2025) adopt hybrid encoders that combine variational autoencoder (VAE Rombach et al. (2022)) latents with Visual Transformer (ViT) features. While this design facilitates generation, it introduces an inherent representational divergence: semantic understanding and image synthesis are grounded in different feature spaces, fundamentally limiting deeper unification. To address this representational schism, some works Geng et al. (2025); Ma et al. (2025a); Han et al. (2025) move toward using only ViT-based visual embeddings, aiming to anchor both understanding and generation within a single semantic space. Within this line of research, some approaches discretize powerful continuous features (e.g., CLIP/SigLIP Radford et al. (2021); Tschannen et al. (2025)) via vector quantization to obtain tractable visual tokens. Although discretization simplifies generative modeling, it inevitably incurs irreversible information loss, particularly in fine-grained spatial and textural details that are essential for high-fidelity image synthesis.

More recent methods Zheng et al. (2025); Tong et al. (2026); Gao et al. (2025); Chen et al. (2025d), abandon quantization altogether and instead operate directly on continuous ViT representations. However, this shift exposes a new challenge: the resulting high-dimensional continuous feature manifold is complex, often non-smooth, and difficult to model generatively (see Fig 9). Therefore, we revisit the visual embeddings from the two perspectives: **modeling and prediction**.

For visual embeddings modeling, we introduce a continuous semantic compressor, a lightweight module that learns to project high-dimensional visual semantics into a compact and continuous latent space. This space serves as a unified representation that preserves essential semantic, structural, and textural information while significantly simplifying the underlying data distribution. We systematically compare different projection strategies and evaluate their reconstruction fidelity, demonstrating that visual embeddings can be compressed in a near-lossless manner. Our

\* Equal contribution. Work done during internship at Tencent Hunyuan.

† Corresponding Authors.

preliminary experiments suggest that such continuous compression preserves both understanding (see Tab 5) and pixel-level reconstruction (see Tab 1) capabilities, while substantially improving training stability and computational efficiency.

Given the compressed representation, we next investigate how to effectively predict visual embeddings from textual conditions. Within a single unified framework, we study and compare two distinct generative pathways. One inspired by Transfusion Zhou et al. (2024) that is trained end-to-end using a unified flow-matching objective over mixed-modality sequences, directly predicting compressed visual latents. Another way introduces a query-based Pan et al. (2025b); Chen et al. (2025b) approach, in which a set of learnable queries is used to extract conditional signals from a powerful multimodal large language model, thereby leveraging its semantic understanding and reasoning capabilities to guide visual generation. Our comparative analysis reveals that the Transfusion pathway achieves faster convergence and maintains stronger consistency in editing tasks. Therefore, we adopt it as the prediction mechanism of our final model.

Finally, we propose **UniCom**, a unified large-scale multimodal model that performs generation directly over compressed visual embeddings. Through systematic analysis, we identify that compressing high-dimensional features along the channel dimension, rather than reducing the token sequence, optimally preserves both semantic fidelity and pixel-level details. The resulting compact representation enables highly efficient and stable training, while our unified prediction pathway achieves state-of-the-art performance across diverse tasks. Notably, UniCom excels in fine-grained text rendering and complex image editing without relying on VAE features for identity preservation, demonstrating that semantically rich and well-compressed visual embeddings can serve as an effective universal interface for both understanding and generation. Our contributions are as follows:

- We establish an effective paradigm for unifying visual understanding and generation by learning to predict continuous, compressed semantic embeddings, which we demonstrate preserves both high-level semantics and fine-grained visual details better than prior quantization methods.
- We revealing that compression along the channel dimension is significantly superior to sequence reduction for preserving information, and that an attention-based projector is crucial for maintaining semantic structure.
- The proposed UniCom model validates this paradigm at scale, achieving state-of-the-art or competitive performance across image reconstruction, text-to-image generation, and challenging image editing tasks.

## 2 Related Work

A prominent approach attempts Team (2024a); Wang et al. (2024); Pan et al. (2025a) to integrate image generation into the autoregressive framework of LLMs, addressing the challenge of image tokenization. Early methods Geng et al. (2025); Gupta et al. (2022); Ma et al. (2025a); Chen et al. (2025f), serialized vision-language encoders like CLIP/SigLIP into token sequences similar to text, typically paired with a diffusion decoder to combine AR understanding with diffusion-based generation. However, the resulting quantization loss and long sequences often lacked the semantic alignment necessary for efficient cross-modal reasoning. Some approaches AI et al. (2025); Tang et al. (2025); Chen et al. (2025b), like MetaQuery Pan et al. (2025b), generate query tokens via an LLM, which are then reconstructed to compact visual representations for image decoding through a diffusion model. Another line of work Shi et al. (2024); Xie et al. (2025b); Ma et al. (2025b); Tong et al. (2026), such as Transfusion Zhou et al. (2024), combines AR’s sequential reasoning with diffusion’s high-fidelity image synthesis. In these models, text tokens are generated autoregressively by an LLM, while image tokens undergo denoising conditioned on the textual context.

## 3 UniCom

### 3.1 Problem Formulation and Unified Framework

Our work posits that the key to a unified and efficient model lies not in circumventing the VLM’s semantic space, but in *transforming it* into a form amenable to generative modeling while preserving its rich informational content. We formulate a two-stage generative process that decomposes the conditional image distribution  $P(\mathbf{x} | \mathbf{c})$  (where  $\mathbf{c}$  is a conditioning context such as text) as follows:

$$P(\mathbf{x} | \mathbf{c}) = \int P(\tilde{\mathbf{z}} | \mathbf{c}) \cdot P(\mathbf{x} | \tilde{\mathbf{z}}) d\tilde{\mathbf{z}}. \quad (1)$$

Here,  $\tilde{\mathbf{z}} \in \mathbb{R}^{N \times d}$  (with  $d \ll D$ ) represents the image in a compressed semantic latent space  $\tilde{\mathcal{Z}}$ . This formulation introduces a critical intermediate variable  $\tilde{\mathbf{z}}$  with two properties:

1. **Semantic Fidelity:**  $\tilde{\mathbf{z}}$  retains the necessary information from  $\mathbf{Z}$  to reconstruct the image  $\mathbf{x}$  with high fidelity, ensuring a strong connection to understanding.

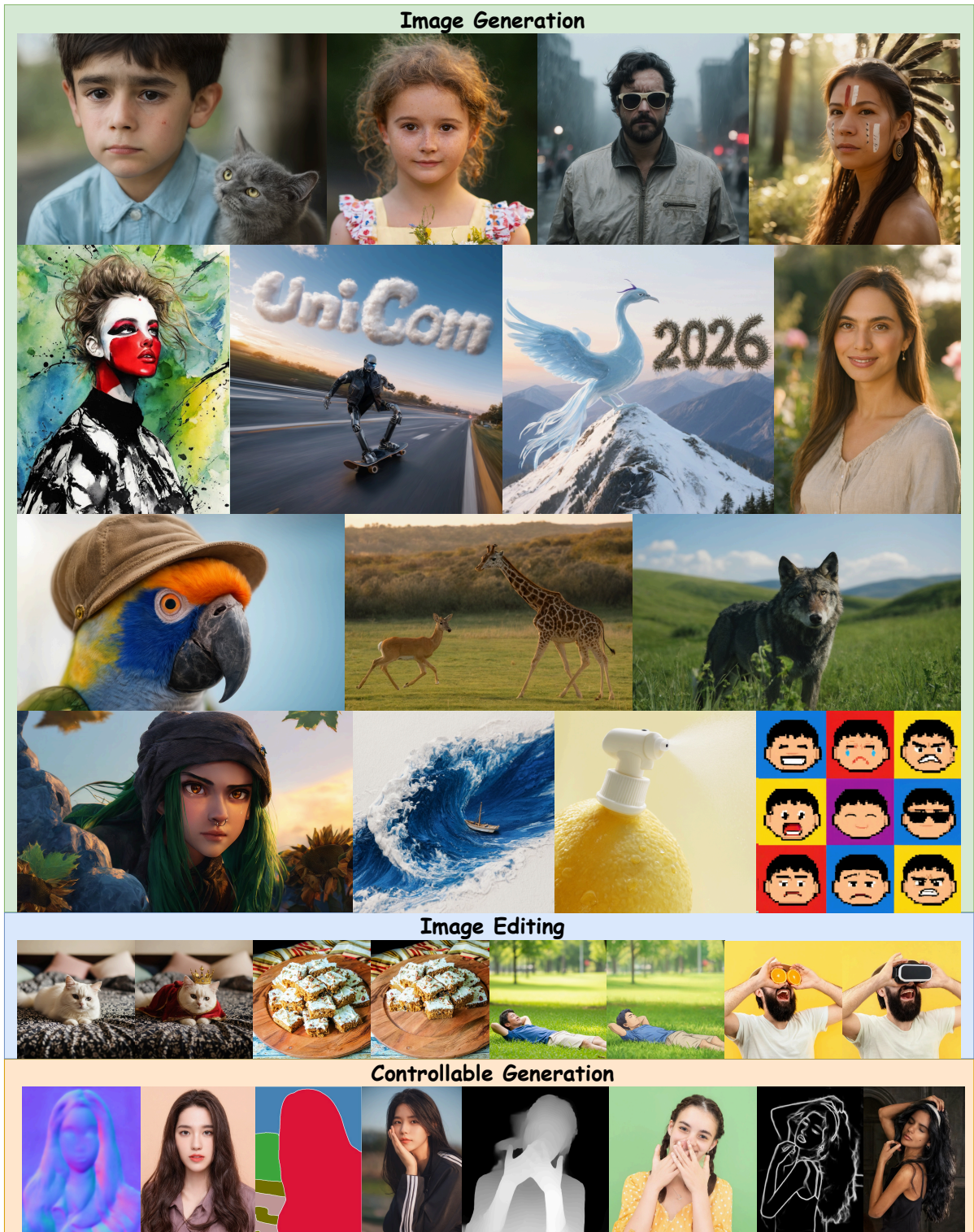


Figure 1: High-quality samples generated by UniCom. Built on compressed continuous representations, our unified multimodal model demonstrates exceptional capabilities in text-to-image generation, precise image editing, and fine-grained controllable generation.

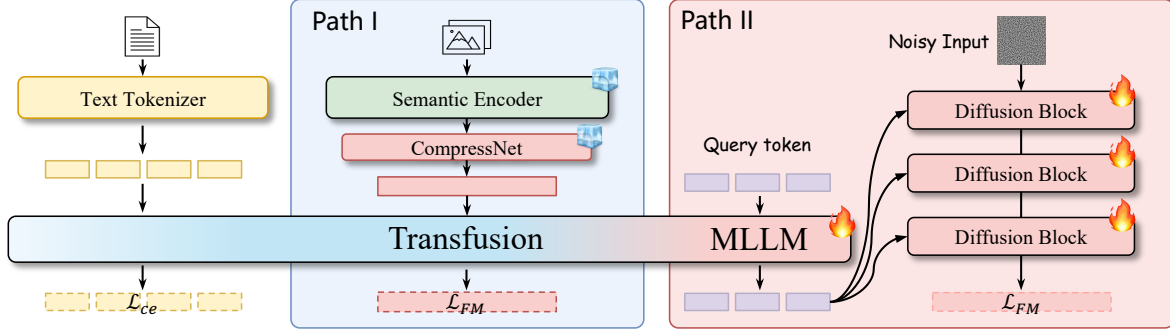


Figure 2: **Overview of the proposed framework.** For a controlled comparison, both pathways are built upon the same compressed representations and jointly optimized with cross-entropy loss ( $\mathcal{L}_{ce}$ ) and flow matching loss ( $\mathcal{L}_{fm}$ ).

2. **Generative Tractability:** The distribution  $P(\tilde{\mathbf{z}} | \mathbf{c})$  over the lower-dimensional space  $\tilde{\mathcal{Z}}$  is significantly smoother for learning and sampling.

Our framework, illustrated in Fig 2, operationalizes this formulation through three core components: Semantic Compressor §3.2, Generative Prior Module §3.3, and Diffusion Decoder. The compressor and decoder are first jointly pre-trained using a reconstruction objective to establish a well-behaved  $\tilde{\mathcal{Z}}$  space. Subsequently, the compressor is frozen, and the Generative Prior Module is trained to sample within this fixed, tractable space.

### 3.2 Semantic Compression and Reconstruction

The core of our framework is the construction of the compressed semantic latent space  $\tilde{\mathcal{Z}}$ . This module must reconcile two competing objectives: **minimizing information loss** to preserve the visual and semantic fidelity required for high-quality reconstruction, and **maximizing tractability** by simplifying the underlying data distribution for robust generative modeling. Formally, we seek a parametric function  $\mathcal{C}_\phi : \mathcal{Z} \rightarrow \tilde{\mathcal{Z}}$  that performs a nonlinear dimensionality reduction, where  $\tilde{\mathcal{Z}} \subset \mathbb{R}^{N \times d}$  and  $d \ll D$ .

**Why Compression is Necessary.** The native VLM embedding space  $\mathcal{Z}$ , while semantically rich, exhibits high dimensionality and a complex, often multi-modal and discontinuous, topology. Directly modeling the distribution  $P(\mathbf{Z} | \mathbf{c})$  with a generative model (e.g., a diffusion process) is empirically unstable and leads to high FID (see Tab 4), as the model struggles to navigate the intricate geometry of  $\mathcal{Z}$ . This observation aligns with the manifold hypothesis; we posit that the information essential for generation lies on a lower-dimensional submanifold within  $\mathcal{Z}$ . The compressor  $\mathcal{C}_\phi$  thus acts as a learned projection that discovers and parameterizes this submanifold.

**Design of the Attention-Based Compressor.** Prior work, such as VUGEN Chen et al. (2025d), employs a simple Multi-Layer Perceptron (MLP) for compression. While effective, an MLP processes each spatial feature token independently, potentially disregarding the crucial long-range contextual relationships between image patches that are inherently captured by the vision encoder’s self-attention layers. To preserve this structured semantic information, we implement  $\mathcal{C}_\phi$  as a shallow, lightweight Transformer module. This design ensures that the mapping is context-aware and permutation-equivariant with respect to the input tokens, preserving the structural semantics of the scene more effectively than an isotropic MLP (see Tab 5 and Fig 8).

**Joint Optimization with the Diffusion Decoder.** The compressor is not trained in isolation. Its parameters  $\phi$  are jointly optimized with the diffusion decoder parameters  $\psi$  using a reconstruction objective. Given an image  $\mathbf{x}$ , its visual features  $\mathbf{Z} = f_{\text{und}}(\mathbf{x})$ , and compressed latents  $\tilde{\mathbf{z}} = \mathcal{C}_\phi(\mathbf{Z})$ , the decoder reconstructs the image as  $\hat{\mathbf{x}} = \mathcal{D}_\psi(\tilde{\mathbf{z}})$ . Training minimizes the composite loss:

$$\mathcal{L}_{\text{recon}} = \mathcal{L}_{\text{flow}}(\mathbf{x}, \hat{\mathbf{x}}) + \lambda \cdot \mathcal{L}_{\text{perc}}(\mathbf{x}, \hat{\mathbf{x}}), \quad (2)$$

where  $\mathcal{L}_{\text{flow}}$  denotes the flow-matching loss used by the diffusion decoder and  $\mathcal{L}_{\text{perc}}$  is a perceptual loss (e.g., LPIPS). This joint training procedure forces  $\mathcal{C}_\phi$  to discard information redundant for pixel-space reconstruction while retaining semantically meaningful and generatively useful signals, thereby shaping  $\tilde{\mathcal{Z}}$  into an *information bottleneck* optimized for generation.

### 3.3 Two Ways of Predicting Representations

With the compressed semantic space  $\tilde{\mathcal{Z}}$  established in Section 3.2, we explore two distinct pathways to model the conditional distribution  $P(\tilde{\mathbf{z}} | \mathbf{c})$ . Both pathways share the same compressor  $\mathcal{C}_\phi$  and diffusion decoder  $\mathcal{D}_\psi$ , ensuring a controlled comparison focused on the prediction mechanism itself.

**Pathway I: Unified Prediction with Transfusion.** This pathway integrates text and image generation within a single, fully trainable transformer model. The model operates on a unified sequence that interleaves discrete text tokens and continuous latent representations of images. Formally, given a text prompt  $\mathbf{c}$ , it is tokenized into a sequence of tokens  $\{\mathbf{w}_1, \dots, \mathbf{w}_L\}$ . To generate an image, we prepend a special [BOI] (Beginning of Image) token and append an [EOI] (End of Image) token to a placeholder sequence of  $N$  latent vectors initialized as pure noise  $\tilde{\mathbf{z}}_T \sim \mathcal{N}(0, I)$ . For visual inputs, the semantic encoder extracts continuous features  $\mathbf{Z} = f_{\text{und}}(\mathbf{x})$ . We directly input the uncompressed  $\mathbf{Z}$  for understanding tasks to preserve fine-grained details, whereas for image editing, we feed the compressed latents  $\tilde{\mathbf{z}} = \mathcal{C}_\phi(\mathbf{Z})$  to reduce context length and facilitate efficient multi-turn editing.

The transformer processes this entire sequence using a modality-aware attention mask. For text tokens, we apply standard causal masking to preserve autoregressive properties. For the latent vectors within the same image (between [BOI] and [EOI]), we employ *bidirectional attention*, allowing all image patches to attend to each other.

**Pathway II: Query-Guided Prediction via an MLLM.** This pathway decouples the understanding and generation roles. We employ a powerful pre-trained MLLM (e.g., Qwen-VL) with its multimodal reasoning and knowledge representation capabilities. To bridge it with the generative diffusion decoder, we introduce a set of learnable parameters called **MetaQueries**, denoted as  $\mathcal{Q} \in \mathbb{R}^{M \times d}$ , where  $M$  is the number of queries and  $d$  matches the MLLM’s hidden dimension.

Given a text condition  $\mathbf{c}$ , we construct the input sequence as the concatenation of the text tokens and the MetaQueries:  $[\mathbf{c}; \mathcal{Q}]$ . This sequence is fed into the frozen MLLM. Through its forward pass, the queries  $\mathcal{Q}$  interact with the text context via the MLLM’s self-attention layers, effectively “querying” the model’s internal knowledge and semantic understanding to produce a conditioned representation. We extract the output states corresponding to the query positions as the conditional signal  $\mathbf{h}_\mathcal{Q} \in \mathbb{R}^{M \times d}$ .

This signal is then projected by a lightweight, trainable connector network (a small transformer encoder) to align it with the input space of the flow-matching decoder, producing the initial condition for the latent representation.

**Flow Matching Training Objective.** During training, given a text condition  $\mathbf{c}$  and its corresponding ground-truth compressed semantic representation  $\tilde{\mathbf{z}}_1$ , we construct training pairs following the standard Flow Matching procedure. Specifically, we sample a time step  $t \sim \mathcal{U}[0, 1]$  and noise  $\epsilon \sim \mathcal{N}(0, I)$ , and compute the interpolated latent

$$\tilde{\mathbf{z}}_t = t\tilde{\mathbf{z}}_1 + (1 - t)\epsilon, \quad (3)$$

along with the target velocity

$$\mathbf{v}_t = \tilde{\mathbf{z}}_1 - \epsilon. \quad (4)$$

The condition  $\mathbf{c}$  and the noised latent  $\tilde{\mathbf{z}}_t$  are assembled into the mixed input sequence and passed through the Transformer. The model predicts the velocity field from the output hidden states corresponding to the positions of  $\tilde{\mathbf{z}}_t$ . Optimization is performed using a mean squared error loss:

$$\mathcal{L}_{\text{FM}} = \mathbb{E}_{t, \mathbf{c}, \tilde{\mathbf{z}}_1, \epsilon} \left[ \|\mathbf{v}_t - \mathbf{v}_\theta(\tilde{\mathbf{z}}_t, t; \mathbf{c})\|_2^2 \right]. \quad (5)$$

During this stage, both the semantic compressor  $\mathcal{C}_\phi$  and the diffusion decoder  $\mathcal{D}_\psi$  are frozen. Consequently, the transformer learns to perform conditional sampling on a fixed, well-structured semantic manifold  $\tilde{\mathcal{Z}}$ .

## 4 Experiments

In this section, we present UniCom, a unified multimodal model via compressed continuous semantic representations. We adopt the Transfusion architecture (Pathway I in Section 3.3) as our default design, which is validated to outperform the Query-Guided alternative in Section 4.4. We describe the implementation details in Section 4.1 and report performance on reconstruction, text-to-image generation, and image editing benchmarks in Section 4.2. In Section 4.3, we ablate the key design choices of our compressed representation, including the optimal feature shape and projector (compressor and decompressor) architecture.

### 4.1 Implementation Details

Our unified model is built upon Qwen-2.5-7B-Instruct Team (2024b) for multimodal understanding

Table 1: **Evaluation on image reconstruction ability on the ImageNet validation set.**  $d$  denotes the feature dimension of compressed representations  $\tilde{\mathbf{z}}$ . Models marked with  $^\dagger$  are re-evaluated using official checkpoints.

Tokenizer	Res.	rFID↓	PSNR↑	SSIM↑
<i>Specialized tokenizers</i>				
SD-VAE Esser et al. (2024b)	256	1.06	28.62	0.86
GigaTok Xiong et al. (2025)	256	0.51	21.32	0.69
VA-VAE Yao et al. (2025)	256	0.26	28.59	0.80
DC-AE Chen et al. (2024)	512	0.22	26.15	0.71
MAE-Tok Chen et al. (2025a)	512	0.62	-	-
TexTok Zha et al. (2025)	512	0.73	24.45	0.66
FLUX.1[dev]-VAE <sup>†</sup> Labs (2024)	512	0.06	33.65	0.93
<i>Unified tokenizers</i>				
UniTok Ma et al. (2025a)	256	0.38	-	-
TokenFlow Qu et al. (2025)	384	0.63	22.77	0.73
X-Omni <sup>†</sup> Chen et al. (2024)	512	8.30	15.66	0.38
MingTok <sup>†</sup> Al et al. (2025)	512	0.53	23.49	0.61
<b>Ours (d64)</b>	1024	0.42	22.28	0.61
<b>Ours (d1152)</b>	1024	0.38	22.60	0.61

Table 2: **Image generation results on GenEval, DPG-Bench, and WISE.** <sup>†</sup> refers to methods using LLM rewriters on GenEval. Abbreviations for WISE: Cult. (Cultural), Bio. (Biology), Phy. (Physics), Chem. (Chemistry).

Models	GenEval							DPG	WISE						
	Single	Two	Count	Colors	Pos	Col-Attr	Overall	Overall	Cult.	Time	Space	Bio.	Phy.	Chem.	Overall
<i>Generation-only Models</i>															
SD3-Medium (Esser et al., 2024a)	0.99	0.94	0.72	0.89	0.33	0.60	0.74	-	-	-	-	-	-	-	-
FLUX.1 [Dev] (Labs, 2024)	0.98	0.93	0.75	0.93	0.68	0.65	0.82	84.00	0.48	<b>0.58</b>	0.62	0.42	0.51	0.35	0.50
<i>Unified Multimodal Models</i>															
MetaQuery-XL <sup>†</sup> (Pan et al., 2025b)	-	-	-	-	-	-	0.80	-	<b>0.56</b>	0.55	0.62	<u>0.49</u>	<u>0.63</u>	<u>0.41</u>	<u>0.55</u>
Tar (Han et al., 2025)	0.99	0.92	<u>0.83</u>	0.85	0.80	0.65	0.84	84.19	-	-	-	-	-	-	-
BLIP3-o (Chen et al., 2025b)	-	-	-	-	-	-	0.84	-	-	-	-	-	-	-	-
UniWorld-V1 <sup>†</sup> (Lin et al., 2025)	0.98	0.93	0.81	0.89	0.74	0.71	0.84	-	0.53	0.55	<b>0.73</b>	0.45	0.59	<u>0.41</u>	<u>0.55</u>
OmniGen2 <sup>†</sup> (Wu et al., 2025b)	0.99	<u>0.96</u>	0.74	<b>0.98</b>	0.71	0.75	0.86	83.57	-	-	-	-	-	-	-
D-DiT (Li et al., 2025)	0.97	<u>0.80</u>	0.54	0.76	0.32	0.50	0.65	-	-	-	-	-	-	-	-
Show-o (Xie et al., 2024)	0.98	0.80	0.66	0.84	0.31	0.50	0.68	-	0.28	0.40	0.48	0.30	0.46	0.30	0.35
Harmon (Wu et al., 2025c)	0.99	0.86	0.66	0.85	0.74	0.48	0.76	-	0.38	0.48	0.52	0.37	0.44	0.29	0.41
MUSE-VL <sup>†</sup> (Xie et al., 2025c)	-	-	-	-	-	-	0.57	-	-	-	-	-	-	-	-
Transfusion (Zhou et al., 2024)	-	-	-	-	-	-	0.63	-	-	-	-	-	-	-	-
Emu3 (Wang et al., 2024)	-	-	-	-	-	-	0.66	81.60	0.34	0.45	0.48	0.41	0.45	0.27	0.39
Show-o2 (Xie et al., 2025b)	<b>1.00</b>	0.87	0.58	0.92	0.52	0.62	0.76	86.14	-	-	-	-	-	-	-
Janus-Pro (Chen et al., 2025e)	0.99	0.89	0.59	0.90	0.79	0.66	0.80	84.19	0.30	0.37	0.49	0.36	0.42	0.26	0.35
Mogao (Liao et al., 2025)	<b>1.00</b>	<b>0.97</b>	<u>0.83</u>	0.93	<u>0.84</u>	<b>0.80</b>	<b>0.89</b>	84.33	-	-	-	-	-	-	-
X-Omni (Geng et al., 2025)	0.98	0.95	0.75	0.91	0.71	0.68	0.83	<b>87.65</b>	-	-	-	-	-	-	-
Ming-UniVision (Huang et al., 2025)	<b>1.00</b>	0.93	0.59	0.93	<b>0.92</b>	0.70	0.85	82.12	-	-	-	-	-	-	-
BAGEL <sup>†</sup> (Deng et al., 2025)	0.98	0.95	<b>0.84</b>	<u>0.95</u>	0.78	<u>0.77</u>	0.88	85.07	0.44	0.55	0.68	0.44	0.60	0.39	0.52
<b>UniCom (Ours)</b>	0.98	0.94	0.81	0.91	0.82	<u>0.77</u>	0.87	85.92	<u>0.55</u>	<u>0.56</u>	<b>0.73</b>	<b>0.58</b>	<b>0.66</b>	<b>0.47</b>	<b>0.58</b>

and FLUX.1-dev Labs (2024) for high-fidelity image generation, utilizing SigLIP2 Tschannen et al. (2025) as the semantic encoder. To effectively bridge the modality gap, we employ a multi-head self-attention compressor for feature compression and a two-layer MLP for visual projection. The training pipeline consists of four progressive stages: alignment, pre-training, continued training, and supervised fine-tuning, all adopting a native-resolution strategy. Please refer to Section A for comprehensive details regarding the decoder architecture, hyperparameter settings, data mixtures, and the ablation setup.

## 4.2 Main Results

**Diffusion Decoder.** We report the quantitative evaluation on the ImageNet validation set Deng et al. (2009) in Tab 1. Notably, comparing the uncompressed (d1152) and compressed (d64) variants, we observe that reducing the channel dimension by  $18\times$  incurs negligible loss in reconstruction fidelity. The qualitative superiority of our approach is further evidenced in Fig 5. As shown in the zoomed-in regions, our method achieves reconstruction fidelity comparable to the specialized Flux VAE, effectively recovering high-frequency details such as small text characters and maintaining consistent facial identity. This stands in sharp contrast to prior methods relying on semantic features, which often exhibit severe degradation in these fine-grained structures. Consistently with recent findings Tong et al. (2026), we observe that incorporating high-quality text-rich data during training is instrumental in enhancing text rendering performance.

**Text to Image Generation.** As shown in Tab 2, on mainstream evaluation benchmarks including GenEval Ghosh et al. (2023) and DPG-Bench Hu et al. (2024), our method achieves performance comparable to state-of-the-art models. Particularly, UniCom achieves outstanding performance on the more challenging Wise Niu et al. (2025) bench. We attribute this advantage primarily to our method’s direct use of visual-semantic features like SigLIP as the learning target. Compared to traditional VAE latent spaces, this semantically rich representation is inherently more suitable for encoding and reconstructing textual semantic information.

**Image Editing.** As shown in Tab 3, our model also demonstrates strong competitiveness in image editing tasks, achieving leading scores on both ImgEdit-Bench Ye et al. (2025) and GEdit-Bench Liu et al. (2025a). Many previous works Tong et al. (2026); Chen et al. (2025d); Gao et al. (2025) that generate based on comprehension priors either rarely systematically evaluate image editing capabilities, or still require introducing the reference image’s VAE latent to maintain identity consistency Chen et al. (2025c). In contrast, our model conditions solely on the text instruction and the semantic features of the reference image, without using any VAE latent. Nonetheless, we still achieve high scores on metrics that measure consistency before and after editing. This strongly proves that our compressed representation can effectively preserve the fine-grained and structural information of the reference image. Notably, on more challenging knowledge-intensive benchmarks such as KRIS-Bench Wu et al. (2025d) and WorldEdit Wang et al. (2026), which require complex world knowledge spanning biology, geography, and cultural understanding, our model achieves the best performance among all open-source models. This demonstrates remarkable capability in handling sophisticated editing scenarios that demand deep semantic comprehension.

Prompt	Input	UniCom	Bagel	GPT4o	Nano Banana	Seedream4.0	FLUX.1Kontext	Step1X-Edit
Remove all the people in the background and change the purple ribbon to orange.								
Remove the cap and give him an afro								
Remove the guy in the blue suit from the image								
Make the man much older								
Add colour to this slide and a line chart showing desired salary increase								
Change the man into a grizzly bear								
Swap the cup of milk and loaf of bread								
Ajust the small card to the size of the large card.								
Action taken by animals in the image to beg for food								
Correct the incorrect sitting posture in the image								

Figure 3: Comparison of the results for image editing, highlighting UniCom performance in tasks such as image manipulation, object swapping, and color adjustment. See more visualization in the Appendix.

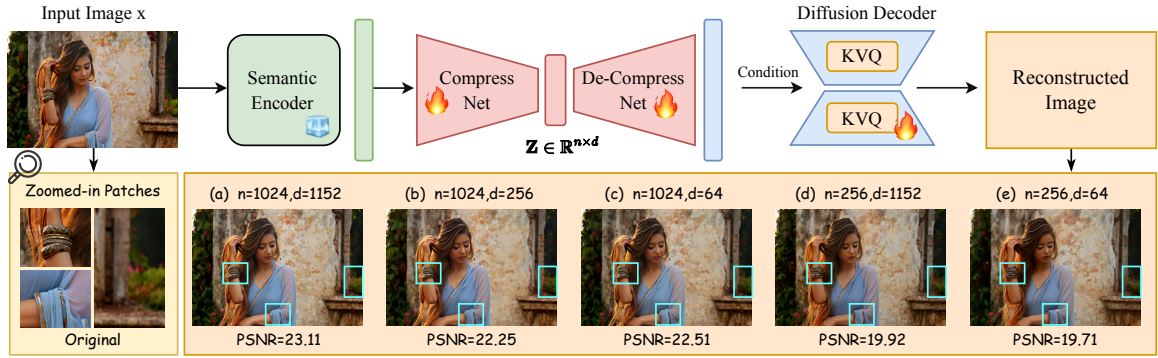


Figure 4: **Overview of the proposed diffusion decoder and reconstruction analysis.** Given an input image, the vision encoder extracts semantic features which are then processed by compressor and decompressor to condition the diffusion model for image reconstruction. During training, the compression modules and the diffusion backbone are optimized, while the encoder remains frozen. We investigate the bottleneck capacity by varying the token number  $n$  and feature dimension  $d$ . As illustrated in the bottom row, compressing the dimension  $d$  yields superior reconstruction fidelity, whereas reducing the token number  $n$  leads to noticeable blurring in fine details.



Figure 5: **Visual comparison of image reconstruction results.** Notably, our method (d64) maintains high fidelity in high-frequency details (e.g., text characters) and preserves facial identity better than these semantic-based baselines, achieving quality comparable to the specialized Flux.1-dev VAE.

### 4.3 Ablation Studies

In this section, we rigorously dissect the design choices for the continuous unified representation  $\tilde{z}$ . We select SigLIP2-SO400M-Patch16-NaFlex Tschannen et al. (2025) features as the foundation due to their dense features for improved semantic understanding. However, directly modeling such high-dimensional representations is challenging. Therefore, we investigate how to efficiently compress these features from two perspectives: (1) Optimal Feature Shape (sequence vs. dimension compression), and (2) Projector Architecture (mlp vs. attention).

#### 4.3.1 Optimal Feature Shape

We first determine the optimal shape for the compressed representation space  $\tilde{z}$  by varying the sequence length  $n$  and feature dimension  $d$ . We control the sequence length  $n$  via the maximum token count and the dimension  $d$  via a learnable mlp bottleneck (compressor and decompressor).

**Reducing dimensions maintains higher reconstruction fidelity than reducing sequence length.** As shown in Tab 4 and Fig 4, original siglip features yield excellent reconstruction fidelity (rFID 0.40). However, reduce sequence

Table 3: **Comparison of image editing capabilities.** We evaluate on ImgEdit-Bench, GEdit-Bench, KRIS-Bench and WorldEdit. For ImgEdit-Bench, performance is evaluated across nine distinct operation categories (e.g., ‘Add’, ‘Adjust’, ‘Extract’, ‘Replace’, ‘Remove’, ‘Background’, ‘Style’, ‘Hybrid’, and ‘Action’). For GEdit-Bench, metrics include ‘G-Semantic Consistency’ (G-SC) and ‘G-Perceptual Quality’ (G-PQ). For KRIS-Bench, we report Factual (Fact.), Conceptual (Conc.), and Procedural (Proc.) knowledge scores. **Bold**: best results. Underline: second-best.

Models	ImgEdit-Bench									GEdit-Bench			KRIS-Bench			WorldEdit		
	Add	Adj.	Ext.	Rep.	Rm.	Bg.	Sty.	Hyb.	Act.	Overall	G-SC	G-PQ	G-Overall	Fact.	Conc.	Proc.	Overall	Overall
<i>Generation-only Models</i>																		
FLUX.1 Kontext [Pro] (Batifol et al., 2025)	4.25	4.15	2.35	4.56	3.57	4.26	4.57	3.68	4.63	4.00	7.02	<u>7.60</u>	6.56	57.22	55.06	46.69	54.17	<u>3.21</u>
Qwen-Image (Wu et al., 2025a)	<u>4.38</u>	<u>4.16</u>	<b>3.43</b>	<u>4.66</u>	4.14	<u>4.38</u>	<b>4.81</b>	<u>3.82</u>	<b>4.69</b>	<u>4.27</u>	<u>8.00</u>	<b>7.86</b>	<b>7.56</b>	-	-	-	-	-
<i>Specialized Editing Models</i>																		
Instruct-Pix2Pix (Brooks et al., 2023)	2.45	1.83	1.44	2.01	1.50	1.44	3.55	1.20	1.46	1.88	3.58	5.49	3.68	23.33	25.59	17.28	22.82	2.44
MagicBrush (Zhang et al., 2023)	2.84	1.58	1.51	1.97	1.58	1.75	2.38	1.62	1.22	1.83	4.68	5.66	4.52	41.84	39.24	26.54	37.15	2.14
AnyEdit (Yu et al., 2025)	3.18	2.95	1.88	2.47	2.23	2.24	2.85	1.56	2.65	2.45	3.18	5.82	3.21	39.26	41.88	31.74	38.55	2.09
Step1X-Edit (Liu et al., 2025a)	3.88	3.14	1.76	3.40	2.41	3.16	4.63	2.64	2.52	3.06	7.09	6.76	6.70	45.52	48.01	31.82	43.29	-
<i>Unified Multimodal Models</i>																		
OmniGen (Xiao et al., 2025)	3.47	3.04	1.71	2.94	2.43	3.21	4.19	2.24	3.38	2.96	5.96	5.89	5.06	33.11	28.02	23.89	28.85	2.52
Ming-Univision (Huang et al., 2025)	-	-	-	-	-	-	-	-	-	-	6.04	6.86	5.54	-	-	-	-	-
BAGEL (Deng et al., 2025)	3.56	3.31	1.70	3.30	2.62	3.24	4.49	2.38	4.17	3.20	7.36	6.83	6.52	<u>60.26</u>	<u>55.86</u>	<u>51.69</u>	<u>56.21</u>	2.76
UniWorld-V1 (Lin et al., 2025)	3.82	3.64	2.27	3.47	3.24	2.99	4.21	2.96	2.74	3.26	4.93	7.43	4.85	-	-	-	-	-
OmniGen2 (Wu et al., 2025b)	3.57	3.06	1.77	3.74	3.20	3.57	<b>4.81</b>	2.52	<u>4.68</u>	3.44	7.16	6.77	6.41	57.36	44.20	47.79	49.71	2.51
TUNA (Liu et al., 2025b)	<b>4.46</b>	<b>4.52</b>	2.47	<b>4.68</b>	<b>4.58</b>	<b>4.56</b>	4.73	<b>4.07</b>	<b>4.69</b>	<b>4.31</b>	7.79	7.48	7.29	-	-	-	-	-
<b>UniCom (Ours)</b>	4.36	4.04	<u>3.30</u>	4.63	<u>4.40</u>	4.24	<u>4.79</u>	3.54	<b>4.69</b>	4.22	<b>8.06</b>	7.33	<u>7.32</u>	<b>74.63</b>	<b>69.48</b>	<b>65.30</b>	<b>70.11</b>	<b>4.12</b>

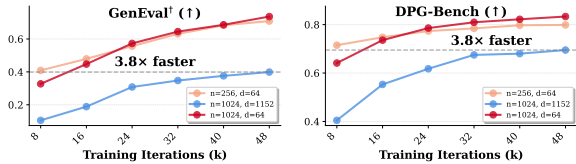


Figure 6: **Feature dimension compression accelerates T2I training.** Compressing to  $d = 64$  achieves  $3.8\times$  faster convergence than original SigLIP features.

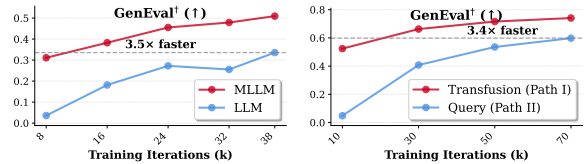


Figure 7: **VLM initialization and Transfusion architecture improve generation.** We report GenEval results during unify pre-training.

length drastically undermines image quality. In contrast, dimension reduction via MLP, whether compressing to 256 or 64 dimensions, results in relatively minimal performance loss.

### Reducing dimensions yields superior image generation performance than reducing sequence length.

Beyond pixel-level reconstruction, we assess how feature shapes impact the generative modeling dynamics of our unified model. As shown in Fig 6, directly modeling uncompressed high-dimensional features ( $d = 1152$ ) results in slow convergence and suboptimal performance. While predicting such high-dimensional targets often requires specific optimization tricks Zheng et al. (2025), these methods may not scale effectively across massive multi-task data. In contrast, compressing the dimension to  $d = 64$  accelerates convergence speed by approximately  $5\times$  and achieves higher final quality. We further observe that maintaining the full token sequence ( $n = 1024$ ) exhibits greater potential in later training stages compared to the token-reduced variant ( $n = 256$ ). Moreover, the high reconstruction fidelity from the full sequence is essential for handling complex editing tasks. Consequently, we select the channel-compressed configuration ( $n = 1024, d = 64$ ) as our optimal training target.

### 4.3.2 Projector Architecture

We compare a simple MLP module against a Multi-Head Attention (MHA) projector inspired by Unitok Ma et al. (2025a). From a reconstruction perspective (Fig 4), both MLP and MHA projectors yield comparable fidelity. However, as our goal is a unified representation, the compressed representations must also retain rich semantic information. We validate this capability through two approaches: feature distribution visualization and downstream understanding benchmarks.

**Distributional Analysis (t-SNE).** We visualize the feature distributions of different encoding strategies in Fig 8. As shown in Fig 8, the MHA projector produces tightly clustered embeddings that maintain the structured distribution of the original SigLIP2 feature. In contrast, the MLP projection results in scattered clusters with blurred semantic boundaries. This suggests that the attention mechanism effectively leverages intra-token context to preserve high-level semantic alignment, whereas the MLP treats tokens in isolation, leading to semantic degradation.

Table 4: Reconstruction performance of different compressed feature shapes on ImageNet50k (Deng et al., 2009).

Projector	Tokens ( $n$ )	Dim ( $d$ )	Reconstruction		
			rFID ↓	PSNR ↑	SSIM ↑
-	1024	1152	0.40	23.26	0.69
-	256	1152	0.72	20.29	0.56
MLP	1024	256	0.62	21.73	0.66
MLP	1024	64	<b>0.55</b>	22.17	0.66
MHA	1024	64	0.56	<b>22.61</b>	<b>0.69</b>

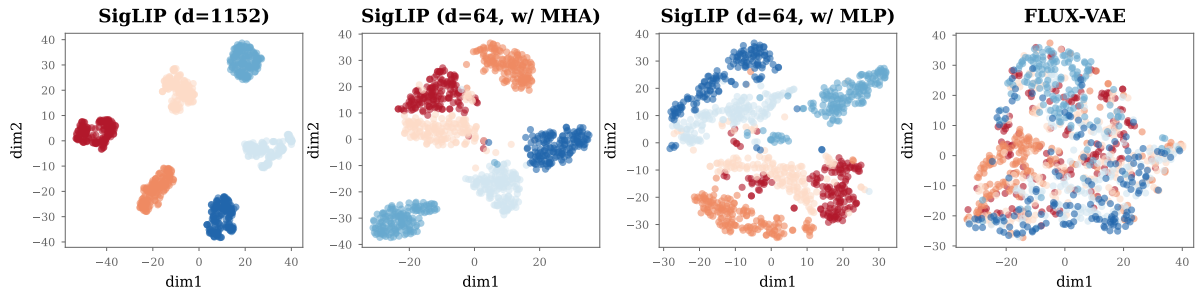


Figure 8: **T-SNE visualization of feature distributions.** We randomly select 6 distinct classes from ImageNet, sampling 150 images per class. MHA compression to 64-d preserves the structure, MLP projection yields scattered 64-d features, and FLUX-VAE has no semantic separability due to pixel-reconstruction focus.

**Downstream Visual Understanding Tasks.** To quantify semantic capability, we employ the compressed representations  $\bar{z}$  within a multimodal LLM framework Liu et al. (2023), pre-training on LLaVA-Pretrain-557k Liu et al. (2023) and fine-tuning on Cambrian-737k Tong et al. (2024). As detailed in Tab 5, the MHA projector consistently outperforms the MLP, confirming that attention-based compression better preserves complex semantics. Although pure compression incurs minor information loss compared to the uncompressed baseline on text-rich tasks, we find that this can be effectively mitigated by fusing the MHA-compressed features with the original siglip features. Specifically, sequence concatenation of these two representations even introduces marginal gains on fine-grained benchmarks. Thus, we adopt the MHA projector as our final design.

Table 5: Visual understanding performance on six benchmarks using compressed representations as visual inputs.

Model Config.	General VQA		Knowledge	Text-Centric		
	GQA	RealWorldQA	SEED	MMMU	ChartQA	OCRBench
Baseline	<b>65.25</b>	64.31	<b>74.63</b>	44.56	69.04	55.40
<i>Compression Strategies</i>						
MLP Proj.	62.80	60.39	69.92	43.00	56.80	31.70
MHA Proj.	64.01	63.14	71.75	44.11	62.12	36.00
<i>Concatenation Strategies</i>						
Dim. Concat	64.22	60.26	73.11	<b>45.00</b>	60.88	48.10
Seq. Concat	65.03	<b>64.58</b>	73.62	43.33	<b>69.24</b>	<b>55.50</b>

#### 4.4 Discussion

**Visual Understanding Inform Image Generation.** To investigate whether the semantic knowledge acquired from understanding tasks contributes to generative performance, we compare two initialization strategies for unified training: (1) Language model from Qwen-2.5-7B Team (2024b), and (2) Pre-trained VLM, where the Qwen-2.5-7B (coupled with SigLIP2 features) was previously trained on image-to-text understanding tasks. Both models are subsequently trained on the unified generation task under identical settings. Fig 7 (Left) compares their training dynamics on the generation task. The *VLM-Base* demonstrates superior performance, characterized by significantly faster convergence and higher final metrics on GenEval and DPG-Bench. This indicates that dense visual-language alignment established during the understanding phase effectively bootstraps the generation process.

**Comparison with Query-Guided Architectures.** We also explored the Query-Guided pathway (Pathway II), inspired by BLIP-3o Chen et al. (2025b). The original design suffers from **feature misalignment**, as the frozen MLLM uses one vision encoder for understanding but is trained to predict features from a different encoder for generation. We addressed this by enforcing a unified feature space with SigLIP2, and further introduced an I2I reconstruction task inspired by RECA Xie et al. (2025a) to improve structural alignment.

Despite these improvements, Pathway II remains inferior to Pathway I. As shown in Fig 7 (Right), the query-based model converges significantly slower during pre-training. Moreover, the query bottleneck discards spatial details, failing to preserve fine-grained layout. In contrast, Pathway I benefits from full-sequence modeling with dense spatial correspondence, yielding superior fidelity and structural consistency in editing (see Fig 12).

## 5 Conclusion

In this paper, we introduce UniCom, a unified multimodal framework that effectively integrates visual understanding and generation by compressing high-dimensional visual embeddings into a compact latent space. Based on the continuous semantic compressor, we explore two distinct generative pathways: Transfusion and MetaQuery. Experimental results show that UniCom not only preserves high-level semantics but also retains fine-grained visual details, achieving significant improvements in text-to-image generation and image editing tasks when compared to existing methods. Furthermore, UniCom demonstrates that compressed semantic representations can be used for both unified generation and understanding without relying on variational autoencoders (VAE). Future work could focus on further optimizing the compression module and expanding the application of this framework to other domains, such as video generation and multimodal reasoning.

---

## References

- Inclusion AI, Biao Gong, Cheng Zou, Chuanyang Zheng, Chunluan Zhou, Canxiang Yan, Chunxiang Jin, Chunjie Shen, Dandan Zheng, Fudong Wang, et al. Ming-omni: A unified multimodal model for perception and generation. *arXiv preprint arXiv:2506.09344*, 2025.
- Stephen Batifol, Andreas Blattmann, Frederic Boesel, Saksham Consul, Cyril Diagne, Tim Dockhorn, Jack English, Zion English, Patrick Esser, Sumith Kulal, et al. Flux. 1 kontekst: Flow matching for in-context image generation and editing in latent space. *arXiv e-prints*, pp. arXiv-2506, 2025.
- Tim Brooks, Aleksander Holynski, and Alexei A Efros. Instructpix2pix: Learning to follow image editing instructions. In *Proceedings of the IEEE/CVF conference on computer vision and pattern recognition*, pp. 18392–18402, 2023.
- Hao Chen, Yujin Han, Fangyi Chen, Xiang Li, Yidong Wang, Jindong Wang, Ze Wang, Zicheng Liu, Difan Zou, and Bhiksha Raj. Masked autoencoders are effective tokenizers for diffusion models. In *Forty-second International Conference on Machine Learning*, 2025a.
- Jiuhai Chen, Zhiyang Xu, Xichen Pan, Yushi Hu, Can Qin, Tom Goldstein, Lifu Huang, Tianyi Zhou, Saining Xie, Silvio Savarese, et al. Blip3-o: A family of fully open unified multimodal models-architecture, training and dataset. *arXiv preprint arXiv:2505.09568*, 2025b.
- Jiuhai Chen, Le Xue, Zhiyang Xu, Xichen Pan, Shusheng Yang, Can Qin, An Yan, Honglu Zhou, Zeyuan Chen, Lifu Huang, et al. Blip3o-next: Next frontier of native image generation. *arXiv preprint arXiv:2510.15857*, 2025c.
- Junyu Chen, Han Cai, Junsong Chen, Enze Xie, Shang Yang, Haotian Tang, Muyang Li, Yao Lu, and Song Han. Deep compression autoencoder for efficient high-resolution diffusion models. *arXiv preprint arXiv:2410.10733*, 2024.
- Xiangyi Chen, Théophane Vallaes, Maha Elbayad, John Nguyen, and Jakob Verbeek. Vugen: Visual understanding priors for generation. *arXiv preprint arXiv:2510.06529*, 2025d.
- Xiaokang Chen, Zhiyu Wu, Xingchao Liu, Zizheng Pan, Wen Liu, Zhenda Xie, Xingkai Yu, and Chong Ruan. Janus-pro: Unified multimodal understanding and generation with data and model scaling. *arXiv preprint arXiv:2501.17811*, 2025e.
- Yanzhe Chen, Huasong Zhong, Yan Li, and Zhenheng Yang. Unicode<sup>2</sup>: Cascaded large-scale codebooks for unified multimodal understanding and generation. *arXiv preprint arXiv:2506.20214*, 2025f.
- Chaurui Deng, Deyao Zhu, Kunchang Li, Chenhui Gou, Feng Li, Zeyu Wang, Shu Zhong, Weihao Yu, Xiaonan Nie, Ziang Song, et al. Emerging properties in unified multimodal pretraining. *arXiv preprint arXiv:2505.14683*, 2025.
- Jia Deng, Wei Dong, Richard Socher, Li-Jia Li, Kai Li, and Li Fei-Fei. Imagenet: A large-scale hierarchical image database. In *2009 IEEE conference on computer vision and pattern recognition*, pp. 248–255. Ieee, 2009.
- Patrick Esser, Robin Rombach, and Bjorn Ommer. Taming transformers for high-resolution image synthesis. In *Proceedings of the IEEE/CVF conference on computer vision and pattern recognition*, pp. 12873–12883, 2021.
- Patrick Esser, Sumith Kulal, Andreas Blattmann, Rahim Entezari, Jonas Müller, Harry Saini, Yam Levi, Dominik Lorenz, Axel Sauer, Frederic Boesel, et al. Scaling rectified flow transformers for high-resolution image synthesis. In *Forty-first international conference on machine learning*, 2024a.
- Patrick Esser, Sumith Kulal, Andreas Blattmann, Rahim Entezari, Jonas Müller, Harry Saini, Yam Levi, Dominik Lorenz, Axel Sauer, Frederic Boesel, Dustin Podell, Tim Dockhorn, Zion English, Kyle Lacey, Alex Goodwin, Yannik Marek, and Robin Rombach. Scaling rectified flow transformers for high-resolution image synthesis, 2024b. URL <https://arxiv.org/abs/2403.03206>.
- Yuan Gao, Chen Chen, Tianrong Chen, and Jiatao Gu. One layer is enough: Adapting pretrained visual encoders for image generation. *arXiv preprint arXiv:2512.07829*, 2025.
- Zigang Geng, Yibing Wang, Yeyao Ma, Chen Li, Yongming Rao, Shuyang Gu, Zhao Zhong, Qinglin Lu, Han Hu, Xiaosong Zhang, et al. X-omni: Reinforcement learning makes discrete autoregressive image generative models great again. *arXiv preprint arXiv:2507.22058*, 2025.
- Dhruba Ghosh, Hannaneh Hajishirzi, and Ludwig Schmidt. Geneval: An object-focused framework for evaluating text-to-image alignment. *Advances in Neural Information Processing Systems*, 36:52132–52152, 2023.
- Agrim Gupta, Linxi Fan, Surya Ganguli, and Li Fei-Fei. Metamorph: Learning universal controllers with transformers. *arXiv preprint arXiv:2203.11931*, 2022.

- 
- Jiaming Han, Hao Chen, Yang Zhao, Hanyu Wang, Qi Zhao, Ziyang Yang, Hao He, Xiangyu Yue, and Lu Jiang. Vision as a dialect: Unifying visual understanding and generation via text-aligned representations. *arXiv preprint arXiv:2506.18898*, 2025.
- Xiwei Hu, Rui Wang, Yixiao Fang, Bin Fu, Pei Cheng, and Gang Yu. Ella: Equip diffusion models with llm for enhanced semantic alignment. *arXiv preprint arXiv:2403.05135*, 2024.
- Ziyuan Huang, DanDan Zheng, Cheng Zou, Rui Liu, Xiaolong Wang, Kaixiang Ji, Weilong Chai, Jianxin Sun, Libin Wang, Yongjie Lv, et al. Ming-univision: Joint image understanding and generation with a unified continuous tokenizer. *arXiv preprint arXiv:2510.06590*, 2025.
- Drew A Hudson and Christopher D Manning. Gqa: A new dataset for real-world visual reasoning and compositional question answering. In *Proceedings of the IEEE/CVF conference on computer vision and pattern recognition*, pp. 6700–6709, 2019.
- Black Forest Labs. Flux.1 model family. <https://blackforestlabs.ai/announcing-black-forest-labs/>, 2024.
- Bohao Li, Rui Wang, Guangzhi Wang, Yuying Ge, Yixiao Ge, and Ying Shan. Seed-bench: Benchmarking multimodal llms with generative comprehension. *arXiv preprint arXiv:2307.16125*, 2023.
- Zijie Li, Henry Li, Yichun Shi, Amir Barati Farimani, Yuval Kluger, Linjie Yang, and Peng Wang. Dual diffusion for unified image generation and understanding. In *Proceedings of the Computer Vision and Pattern Recognition Conference*, pp. 2779–2790, 2025.
- Chao Liao, Liyang Liu, Xun Wang, Zhengxiong Luo, Xinyu Zhang, Wenliang Zhao, Jie Wu, Liang Li, Zhi Tian, and Weilin Huang. Mogao: An omni foundation model for interleaved multi-modal generation. *arXiv preprint arXiv:2505.05472*, 2025.
- Bin Lin, Zongjian Li, Xinhua Cheng, Yuwei Niu, Yang Ye, Xianyi He, Shenghai Yuan, Wangbo Yu, Shaodong Wang, Yongyang Ge, et al. Uniworld: High-resolution semantic encoders for unified visual understanding and generation. *arXiv preprint arXiv:2506.03147*, 2025.
- Haotian Liu, Chunyuan Li, Qingyang Wu, and Yong Jae Lee. Visual instruction tuning. *Advances in neural information processing systems*, 36:34892–34916, 2023.
- Shiyu Liu, Yucheng Han, Peng Xing, Fukun Yin, Rui Wang, Wei Cheng, Jiaqi Liao, Yingming Wang, Honghao Fu, Chunrui Han, Guopeng Li, Yuang Peng, Quan Sun, Jingwei Wu, Yan Cai, Zheng Ge, Ranchen Ming, Lei Xia, Xianfang Zeng, Yibo Zhu, Binxing Jiao, Xiangyu Zhang, Gang Yu, and Daxin Jiang. Step1x-edit: A practical framework for general image editing. *arXiv preprint arXiv:2504.17761*, 2025a.
- Yuliang Liu, Zhang Li, Mingxin Huang, Biao Yang, Wenwen Yu, Chunyuan Li, Xu-Cheng Yin, Cheng-Lin Liu, Lianwen Jin, and Xiang Bai. Ocrbench: on the hidden mystery of ocr in large multimodal models. *Science China Information Sciences*, 67(12):220102, 2024.
- Zhiheng Liu, Weiming Ren, Haozhe Liu, Zijian Zhou, Shoufa Chen, Haonan Qiu, Xiaoke Huang, Zhaochong An, Fanny Yang, Aditya Patel, et al. Tuna: Taming unified visual representations for native unified multimodal models. *arXiv preprint arXiv:2512.02014*, 2025b.
- Chuofan Ma, Yi Jiang, Junfeng Wu, Jihan Yang, Xin Yu, Zehuan Yuan, Bingyue Peng, and Xiaojuan Qi. Unitok: A unified tokenizer for visual generation and understanding. *arXiv preprint arXiv:2502.20321*, 2025a.
- Yiyang Ma, Xingchao Liu, Xiaokang Chen, Wen Liu, Chengyue Wu, Zhiyu Wu, Zizheng Pan, Zhenda Xie, Haowei Zhang, Xingkai Yu, et al. Janusflow: Harmonizing autoregression and rectified flow for unified multimodal understanding and generation. In *Proceedings of the Computer Vision and Pattern Recognition Conference*, pp. 7739–7751, 2025b.
- Ahmed Masry, Xuan Long Do, Jia Qing Tan, Shafiq Joty, and Enamul Hoque. Chartqa: A benchmark for question answering about charts with visual and logical reasoning. In *Findings of the association for computational linguistics: ACL 2022*, pp. 2263–2279, 2022.
- Yuwei Niu, Munan Ning, Mengren Zheng, Weiyang Jin, Bin Lin, Peng Jin, Jiaqi Liao, Chaoran Feng, Kunpeng Ning, Bin Zhu, et al. Wise: A world knowledge-informed semantic evaluation for text-to-image generation. *arXiv preprint arXiv:2503.07265*, 2025.
- Kaihang Pan, Wang Lin, Zhongqi Yue, Tenglong Ao, Liyu Jia, Wei Zhao, Juncheng Li, Siliang Tang, and Hanwang Zhang. Generative multimodal pretraining with discrete diffusion timestep tokens. In *Proceedings of the Computer Vision and Pattern Recognition Conference*, pp. 26136–26146, 2025a.

- 
- Xichen Pan, Satya Narayan Shukla, Aashu Singh, Zhuokai Zhao, Shlok Kumar Mishra, Jialiang Wang, Zhiyang Xu, Jiuhai Chen, Kungpeng Li, Felix Juefei-Xu, et al. Transfer between modalities with metaqueries. *arXiv preprint arXiv:2504.06256*, 2025b.
- Liao Qu, Huichao Zhang, Yiheng Liu, Xu Wang, Yi Jiang, Yiming Gao, Hu Ye, Daniel K Du, Zehuan Yuan, and Xinglong Wu. Tokenflow: Unified image tokenizer for multimodal understanding and generation. In *Proceedings of the Computer Vision and Pattern Recognition Conference*, pp. 2545–2555, 2025.
- Alec Radford, Jong Wook Kim, Chris Hallacy, Aditya Ramesh, Gabriel Goh, Sandhini Agarwal, Girish Sastry, Amanda Askell, Pamela Mishkin, Jack Clark, et al. Learning transferable visual models from natural language supervision. In *International conference on machine learning*, pp. 8748–8763. PmLR, 2021.
- Robin Rombach, Andreas Blattmann, Dominik Lorenz, Patrick Esser, and Björn Ommer. High-resolution image synthesis with latent diffusion models. In *Proceedings of the IEEE/CVF conference on computer vision and pattern recognition*, pp. 10684–10695, 2022.
- Weijia Shi, Xiaochuang Han, Chunting Zhou, Weixin Liang, Xi Victoria Lin, Luke Zettlemoyer, and Lili Yu. Lmfusion: Adapting pretrained language models for multimodal generation. *arXiv preprint arXiv:2412.15188*, 2024.
- Hao Tang, Chenwei Xie, Xiaoyi Bao, Tingyu Weng, Pandeng Li, Yun Zheng, and Liwei Wang. Unilip: Adapting clip for unified multimodal understanding, generation and editing. *arXiv preprint arXiv:2507.23278*, 2025.
- Chameleon Team. Chameleon: Mixed-modal early-fusion foundation models. *arXiv preprint arXiv:2405.09818*, 2024a.
- Qwen Team. Qwen2.5: A party of foundation models, September 2024b. URL <https://qwenlm.github.io/blog/qwen2.5/>.
- Peter Tong, Ellis Brown, Penghao Wu, Sanghyun Woo, Adithya Jairam Vedagiri IYER, Sai Charitha Akula, Shusheng Yang, Jihan Yang, Manoj Middepogu, Ziteng Wang, et al. Cambrian-1: A fully open, vision-centric exploration of multimodal llms. *Advances in Neural Information Processing Systems*, 37:87310–87356, 2024.
- Shengbang Tong, Boyang Zheng, Ziteng Wang, Bingda Tang, Nanye Ma, Ellis Brown, Jihan Yang, Rob Fergus, Yann LeCun, and Saining Xie. Scaling text-to-image diffusion transformers with representation autoencoders. *arXiv preprint arXiv:2601.16208*, 2026.
- Michael Tschannen, Alexey Gritsenko, Xiao Wang, Muhammad Ferjad Naeem, Ibrahim Alabdulmohsin, Nikhil Parthasarathy, Talfan Evans, Lucas Beyer, Ye Xia, Basil Mustafa, Olivier Hénaff, Jeremiah Harmsen, Andreas Steiner, and Xiaohua Zhai. Siglip 2: Multilingual vision-language encoders with improved semantic understanding, localization, and dense features, 2025. URL <https://arxiv.org/abs/2502.14786>.
- Lin Wang, Feng Wang, Majun Zhang, Wentao Hu, Tao Jin, Zhou Zhao, Fei Wu, Jingyuan Chen, Sucheng Ren, and Alan Yuille. Worldedit: Towards open-world image editing with a knowledge-informed benchmark. In *ICLR*, 2026.
- Peiyu Wang, Yi Peng, Yimeng Gan, Liang Hu, Tianyidan Xie, Xiaokun Wang, Yichen Wei, Chuanxin Tang, Bo Zhu, Changshi Li, et al. Skywork unipic: Unified autoregressive modeling for visual understanding and generation. *arXiv preprint arXiv:2508.03320*, 2025.
- Xinlong Wang, Xiaosong Zhang, Zhengxiong Luo, Quan Sun, Yufeng Cui, Jinsheng Wang, Fan Zhang, Yueze Wang, Zhen Li, Qiyong Yu, et al. Emu3: Next-token prediction is all you need. *arXiv preprint arXiv:2409.18869*, 2024.
- Chenfei Wu, Jiahao Li, Jingren Zhou, Junyang Lin, Kaiyuan Gao, Kun Yan, Sheng-ming Yin, Shuai Bai, Xiao Xu, Yilei Chen, et al. Qwen-image technical report. *arXiv preprint arXiv:2508.02324*, 2025a.
- Chenyuan Wu, Pengfei Zheng, Ruiran Yan, Shitao Xiao, Xin Luo, Yueze Wang, Wanli Li, Xiyan Jiang, Yexin Liu, Junjie Zhou, et al. Omnigen2: Exploration to advanced multimodal generation. *arXiv preprint arXiv:2506.18871*, 2025b.
- Size Wu, Wenwei Zhang, Lumin Xu, Sheng Jin, Zhonghua Wu, Qingyi Tao, Wentao Liu, Wei Li, and Chen Change Loy. Harmonizing visual representations for unified multimodal understanding and generation. *arXiv preprint arXiv:2503.21979*, 2025c.
- Yongliang Wu, Zonghui Li, Xinting Hu, Xinyu Ye, Xianfang Zeng, Gang Yu, Wenbo Zhu, Bernt Schiele, Ming-Hsuan Yang, and Xu Yang. Kris-bench: Benchmarking next-level intelligent image editing models. *arXiv preprint arXiv:2505.16707*, 2025d.
- xAI. Grok-1.5 vision preview, 2024. URL <https://x.ai/news/grok-1.5v>. Company news post.

- 
- Shitao Xiao, Yueze Wang, Junjie Zhou, Huaying Yuan, Xingrun Xing, Ruiran Yan, Chaofan Li, Shuting Wang, Tiejun Huang, and Zheng Liu. Omnigen: Unified image generation. In *Proceedings of the Computer Vision and Pattern Recognition Conference*, pp. 13294–13304, 2025.
- Ji Xie, Trevor Darrell, Luke Zettlemoyer, and XuDong Wang. Reconstruction alignment improves unified multimodal models. *arXiv preprint arXiv:2509.07295*, 2025a.
- Jinheng Xie, Weijia Mao, Zechen Bai, David Junhao Zhang, Weihao Wang, Kevin Qinghong Lin, Yuchao Gu, Zhijie Chen, Zhenheng Yang, and Mike Zheng Shou. Show-o: One single transformer to unify multimodal understanding and generation. *arXiv preprint arXiv:2408.12528*, 2024.
- Jinheng Xie, Zhenheng Yang, and Mike Zheng Shou. Show-o2: Improved native unified multimodal models. *arXiv preprint arXiv:2506.15564*, 2025b.
- Rongchang Xie, Chen Du, Ping Song, and Chang Liu. Muse-vl: Modeling unified vlm through semantic discrete encoding. In *Proceedings of the IEEE/CVF International Conference on Computer Vision*, pp. 24135–24146, 2025c.
- Tianwei Xiong, Jun Hao Liew, Zilong Huang, Jiashi Feng, and Xihui Liu. Gigatok: Scaling visual tokenizers to 3 billion parameters for autoregressive image generation. *arXiv preprint arXiv:2504.08736*, 2025.
- Jingfeng Yao, Bin Yang, and Xinggang Wang. Reconstruction vs. generation: Taming optimization dilemma in latent diffusion models. In *Proceedings of the Computer Vision and Pattern Recognition Conference*, pp. 15703–15712, 2025.
- Yang Ye, Xianyi He, Zongjian Li, Bin Lin, Shenghai Yuan, Zhiyuan Yan, Bohan Hou, and Li Yuan. Imgedit: A unified image editing dataset and benchmark. *arXiv preprint arXiv:2505.20275*, 2025.
- Qifan Yu, Wei Chow, Zhongqi Yue, Kaihang Pan, Yang Wu, Xiaoyang Wan, Juncheng Li, Siliang Tang, Hanwang Zhang, and Yueting Zhuang. Anyedit: Mastering unified high-quality image editing for any idea. In *Proceedings of the Computer Vision and Pattern Recognition Conference*, pp. 26125–26135, 2025.
- Xiang Yue, Yuansheng Ni, Kai Zhang, Tianyu Zheng, Ruoqi Liu, Ge Zhang, Samuel Stevens, Dongfu Jiang, Weiming Ren, Yuxuan Sun, et al. Mmmu: A massive multi-discipline multimodal understanding and reasoning benchmark for expert agi. In *Proceedings of the IEEE/CVF Conference on Computer Vision and Pattern Recognition*, pp. 9556–9567, 2024.
- Kaiwen Zha, Lijun Yu, Alireza Fathi, David A Ross, Cordelia Schmid, Dina Katabi, and Xiuye Gu. Language-guided image tokenization for generation. In *Proceedings of the Computer Vision and Pattern Recognition Conference*, pp. 15713–15722, 2025.
- Kai Zhang, Lingbo Mo, Wenhui Chen, Huan Sun, and Yu Su. Magicbrush: A manually annotated dataset for instruction-guided image editing. In *NeurIPS*, 2023.
- Boyang Zheng, Nanye Ma, Shengbang Tong, and Saining Xie. Diffusion transformers with representation autoencoders. *arXiv preprint arXiv:2510.11690*, 2025.
- Chunting Zhou, Lili Yu, Arun Babu, Kushal Tirumala, Michihiro Yasunaga, Leonid Shamis, Jacob Kahn, Xuezhe Ma, Luke Zettlemoyer, and Omer Levy. Transfusion: Predict the next token and diffuse images with one multi-modal model. *arXiv preprint arXiv:2408.11039*, 2024.

---

## A Implementation details

### A.1 Decoder Setup.

As illustrated in Figure 4, we employ the SigLIP2-SO400M-Patch16-NaFlex Tschannen et al. (2025) as our vision encoder. To enable high-fidelity image generation, we initialize the diffusion backbone with FLUX.1-dev Labs (2024). Crucially, to bridge the dimensionality gap between dense semantic features and the generative latent space, we implement a multi-head self-attention mechanism following UniTok Ma et al. (2025a), which effectively preserves rich semantics during feature compression. We optimize both the compression module and the diffusion model on a high-quality internal dataset. We adopt a robust multi-resolution training strategy. Specifically, we define a grid of 33 discrete aspect ratio buckets, ranging from 1:4 (vertical) to 4:1 (horizontal), anchored at a base resolution of  $1024 \times 1024$ . Training is conducted with a global batch size of 256. We observe rapid convergence, achieving high-quality reconstruction performance within 10K steps. However, we extend training to a total of 50K steps to ensure the full recovery of fine-grained visual details.

### A.2 Unified Model Setup.

We initialize the language component with Qwen2.5-7B-Instruct Team (2024b) and the vision encoder with SigLIP2-SO400M-Patch16-NaFlex Tschannen et al. (2025). Visual features are projected into the LLM’s embedding space via a two-layer MLP projector. As outlined in Table 6, we employ a multi-stage training pipeline using a dynamic mixture of curated data. Throughout all phases, we keep the SigLIP2 vision encoder frozen and adopt the same multi-resolution strategy utilized in the decoder setup, processing images with dynamic token counts up to a maximum of 1,024. The training process proceeds as follows: (1) **Alignment**: We establish fundamental visual understanding capabilities by optimizing both the MLP connector and the language model parameters. (2) **Pre-training**: Subsequently, we inject generative capabilities using a massive corpus of text, image-text pairs, and image-text-image sequences. (3) **Continued Training**: To enhance performance on complex tasks such as inpainting and subject-driven generation, we strategically increase the sampling ratio of image-text-image pairs. (4) **Supervised Fine-tuning**: Finally, the model undergoes fine-tuning on high-quality curated data to ensure precise instruction following across all modalities.

### A.3 Ablation Setup.

For efficient ablation analysis in Section 4.3, we switch to reduced data scales and simple task configurations. When investigating reconstruction fidelity, we train the compression and diffusion modules on a subset of high-quality internal images. Regarding generative modeling dynamics, we train the model on a filtered text-to-image dataset to assess convergence speed and generation quality. We evaluate the model’s multimodal understanding capabilities on multiple benchmarks, including general VQA benchmarks such as GQA Hudson & Manning (2019), RealWorldQA xAI (2024), and SEED-Bench Li et al. (2023); knowledge-intensive benchmarks such as MMMU (Yue et al., 2024); and text-centric benchmarks including ChartQA Masry et al. (2022), OCRBench Liu et al. (2024).

## B Related Work

The visual tokenizer Pan et al. (2025a); Ma et al. (2025a); Han et al. (2025) stands as a cornerstone in the realization of unified multimodal models. Its paramount function resides in transmuting visual imagery into visual tokens amenable to processing by generative models, thereby facilitating the concurrent support of both image understanding and generation tasks. Traditional visual generation has long been predicated on pixel-based encoders rooted in Variational Autoencoders (VAEs Rombach et al. (2022)), which affect image generation by projecting visual data into a low-dimensional latent space. Nevertheless, such pixel-centric encoders are often deficient in high-level semantic features and fail to adequately harness the priors inherent in visual understanding, a limitation that constrains their performance in generative endeavors. To remediate this shortcoming, several lines of research Chen et al. (2025e); Wang et al. (2025); Qu et al. (2025); Xie et al. (2025b); Deng et al. (2025) have advanced Hybrid Encoding methodologies, which integrate pixel encoding (VAE) with Transformer-based Vision Transformer (ViT) models in a bid to unify image generation and understanding. Yet, this approach remains flawed: generation and understanding tasks still operate within disparate representational spaces, engendering a disjunction between the two and compromising overall efficiency.

More sophisticated paradigms pivot toward ViT-based visual tokenizers Geng et al. (2025); Ma et al. (2025a); Han et al. (2025). For instance, Vector Quantization (VQ)-based methods Esser et al. (2021) generate discrete visual tokens by quantizing continuous ViT features. While such approaches can effectively convey image information to generative models, the quantization process inevitably incurs information loss, and discrete token systems struggle to articulate the nuanced complexities of intricate visual features. By way of contrast, recent work has gravitated toward the employment of continuous ViT features for visual representation, exemplified by frameworks such as

MingTok Huang et al. (2025) and VUGEN Chen et al. (2025d). These methodologies eschew the discretization process; by adopting continuous visual representations, they succeed in unifying understanding and generation tasks within a shared representational space. They surmount the twin pitfalls of information loss and task disjunction that plagued traditional methods, thereby elevating both the quality and diversity of generated images.

## C Impact of Dimensionality Compression on Training

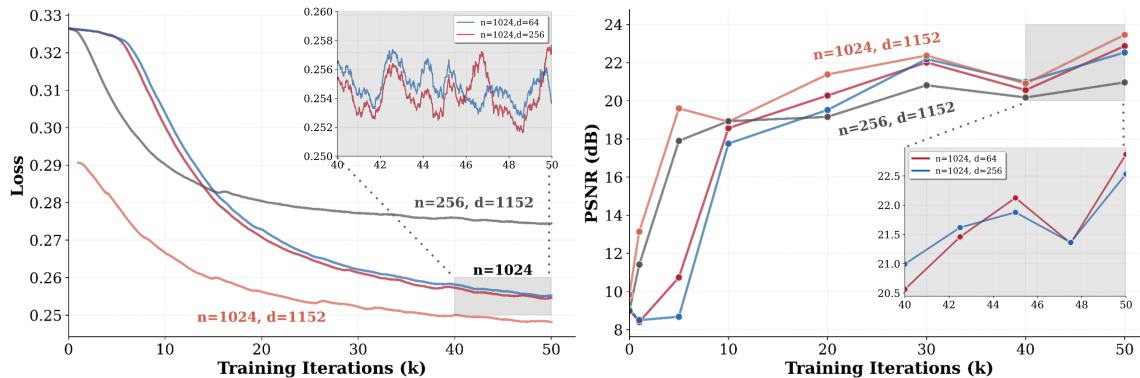


Figure 9: **Reducing dimensions maintains higher reconstruction fidelity than sequence reduction.** We compare the reconstruction training dynamics (Loss and PSNR) of different compressed representations ( $\tilde{z}$ ).

Figure 9 further illustrates that while dimension compression exhibits slower initial convergence compared to the sequence variant (step < 10K), it rapidly matches the capability of the uncompressed baseline. Notably, we observe that as data and compute scale, the performance gap becomes negligible. This suggests that the dense semantic features are highly compressible along the channel dimension without sacrificing pixel details.

## D More Reconstruction Results

We provide comprehensive qualitative evaluations in Figure 10 and Figure 11. As illustrated in Figure 10, prior unified tokenizers relying on semantic encoders often struggle with high-frequency details, resulting in blurred text and distorted small objects. In contrast, our approach preserves these fine-grained structures with high precision. Furthermore, Figure 11 presents a direct side-by-side comparison between our channel-compressed reconstructions (d64) and the original images. The results demonstrate that our method retains intricate details, such as fabric textures, lighting gradients, and clothing lettering, rendering the reconstructed images perceptually indistinguishable from the ground truth.

## E More Results of Image Editing

We present comprehensive qualitative results to demonstrate the versatility of UniCom across diverse image editing and generation scenarios, spanning single-image editing (Figure 13), multi-element composition (Figure 14), and knowledge-driven intelligent editing (Figure 15).

**Single Image Editing.** Figure 13 illustrates the broad editing capabilities of UniCom across six representative tasks: (1) *Add/Remove/Extract*, which covers adding objects, removing elements, and extracting subjects from scenes; (2) *Replace*, which substitutes objects or materials while faithfully preserving contextual layout; (3) *Style Transfer*, which transforms image appearance into various artistic styles; (4) *Background*, which modifies or replaces image backgrounds; (5) *Subject-Driven Generation*, which generates new images conditioned on reference subjects; and (6) *Controllable Generation*, which produces images guided by spatial or structural control signals. These results confirm that our compressed continuous semantic representation retains sufficient fine-grained information to enable precise, instruction-following edits.

**Multi-Element Composition.** Figure 14 demonstrates the ability of UniCom to compose multiple reference subjects into a coherent scene. Despite the challenge of maintaining the identity of each element while harmonizing spatial arrangement and stylistic consistency, our model produces visually plausible compositions. This capability benefits from the rich semantic priors preserved by the channel-compressed representation, enabling faithful identity preservation even without relying on VAE-based reconstruction.

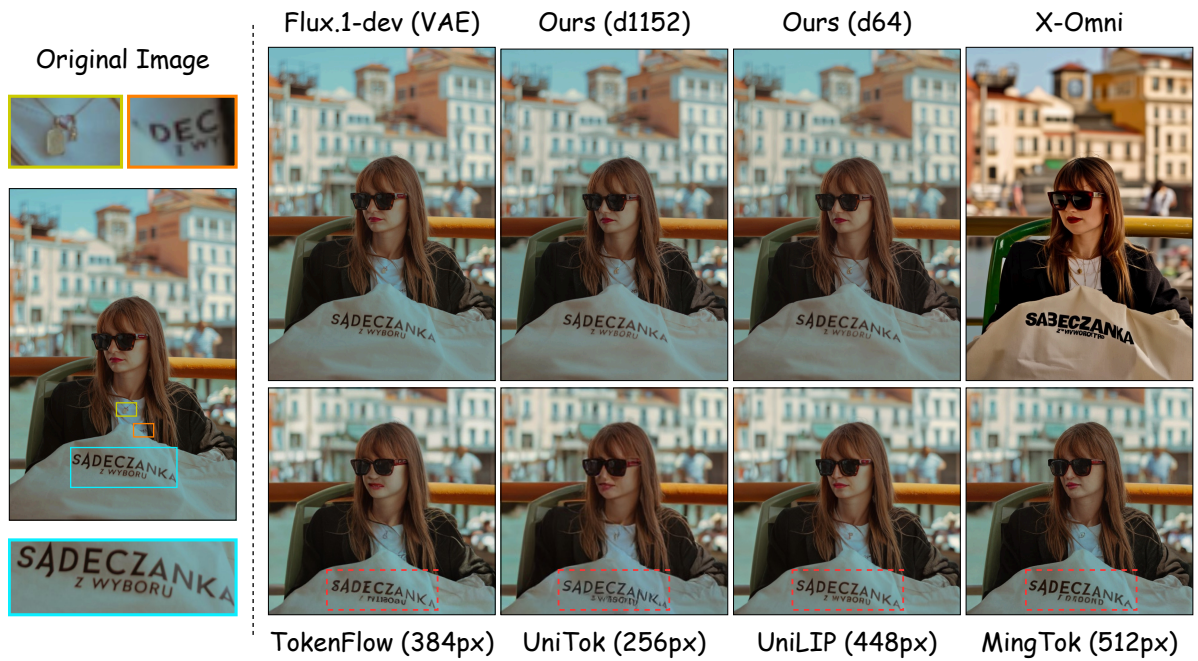


Figure 10: Additional visual comparison of image reconstruction results.



Figure 11: **Qualitative reconstruction samples using Decoder (d64).** **Left:** Reconstructed image. **Right:** Original image. Even with an  $18\times$  channel compression ratio, our model accurately recovers complex high-frequency details.

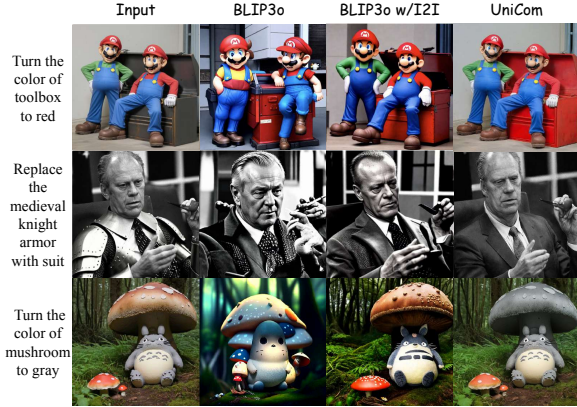


Figure 12: Our unified prediction architecture (*UniCom*) preserves finer spatial layout and structural consistency, while query-based methods struggle with spatial correspondence and editing fidelity.

**Intelligent Image Editing.** Beyond conventional instruction-based editing, we further evaluate UniCom on benchmarks that require world knowledge and contextual reasoning, namely WorldEdit Wang et al. (2026) and Kris Wu et al. (2025d). Unlike systems that rely on explicit editing commands, these benchmarks require models to integrate world knowledge priors and perform reasoning over semantic representations before generating the desired output. Figure 15 showcases representative examples that involve biological transformations, geographical understanding, and cultural context. Rather than following literal instructions, the model must infer what transformation is semantically appropriate given the input, which highlights the advantage of unifying understanding and generation within a shared semantic space.

Quantitatively, as shown in Table 7, UniCom achieves a high overall score of 4.35/5 on WorldEdit-Test, demonstrating strong performance across diverse cause categories. These results underscore the effectiveness of semantic representation for generation: by leveraging rich visual-language priors, UniCom produces more coherent and contextually accurate edits, outperforming most traditional methods that rely solely on explicit instructions. The integration of world knowledge and reasoning significantly enhances the model’s ability to handle complex and context-sensitive editing tasks.

## F Chain-of-Thought Enhanced Generation

To further improve the quality and controllability of image editing and generation, we incorporate chain-of-thought (CoT) reasoning into the training pipeline of UniCom. Specifically, during training, we enable CoT for a proportion of samples by prepending a `<think>` token before the output image. This encourages the model to first produce a structured reasoning trace that plans the visual transformation, and then generate the target image conditioned on both the original input and the reasoning content.

Figure 16 presents representative examples where CoT is activated during inference. For each case, we display the generated image alongside the corresponding thinking process. As shown, the model explicitly reasons about the required modifications (e.g., identifying which attributes to change, understanding spatial relationships, or decomposing complex instructions into sub-steps) before producing the output. This explicit reasoning step enables more accurate and semantically faithful generation, particularly for tasks that involve multi-step transformations or require fine-grained control over the output.

## G Limitation

While UniCom represents a significant step forward in unifying visual understanding and generation, there are still several limitations that need to be addressed. One primary limitation is the complexity involved in training high-dimensional continuous representations. Despite the success of our compression techniques, there is still potential for information loss during the compression process, particularly when dealing with very fine-grained details in complex images. While we have demonstrated the ability of UniCom to preserve these details, the trade-off between compression and fidelity remains a challenging aspect of our approach.

Another limitation arises from the inherent challenges of training generative models, UniCom still requires substantial computational resources, especially for large-scale datasets and high-resolution image tasks. The energy

Table 6: Training hyperparameters and datasets.

	Alignment	PT	CT	SFT
<b>Hyperparameters</b>				
Learning rate	$2.0 \times 10^{-5}$	$1.0 \times 10^{-4}$	$1.0 \times 10^{-4}$	$1.0 \times 10^{-5}$
LR scheduler	Cosine	Constant	Constant	Constant
Weight decay	0.0	0.01	0.01	0.01
Gradient norm clip	1.0	1.0	1.0	1.0
Optimizer	AdamW ( $\beta_1=0.9, \beta_2=0.95, \epsilon=10^{-6}$ )			
Loss weight ( $\lambda_{\text{diff}}:\lambda_{\text{text}}$ )	-	5:1	5:1	5:1
Warm-up steps	600	5000	5000	100
Training steps	20K	115K	60K	7K
<b>Data sampling ratio</b>				
Text-only	0.2	0.25	0.20	0.10
Image-Text (T2I)	0.0	0.45	0.40	0.20
Image-Text (I2T)	0.8	0.15	0.20	0.40
Image-Text-Image	0.0	0.15	0.20	0.30

Table 7: The performance of both commercial and open-source models on image editing tasks in WorldEdit-Test, evaluated across different causes and metrics.

Cause Category	Metric	GPT-4o	Nano-Banana	Seedream4.0	UniCom	WorldEdit	Flux-Kontext	Bagel-Think	Bagel	Omnigen	Omnigen2	Emu2	Anyedit	Ip2p	Magicbrush
Time	VC	4.02	4.22	3.92	3.08	4.18	4.6	2.38	2.34	3.02	2.22	1.48	1.63	3.04	1.40
	VQ	5.00	5.00	4.86	4.78	4.55	4.88	4.52	4.02	4.20	4.35	4.56	3.25	4.51	4.28
	IF	3.86	3.90	4.25	4.08	3.71	1.46	2.46	1.66	1.38	1.33	1.54	1.79	1.51	1.19
	KP	4.20	4.14	4.41	4.38	3.94	1.42	2.86	1.80	1.48	1.25	1.75	1.92	1.65	1.34
	Avg	4.27	4.32	4.36	4.08	4.10	3.09	3.06	2.46	2.52	2.29	2.33	2.15	2.68	2.05
Temperature	VC	4.02	4.22	4.06	3.40	3.52	3.86	2.08	1.94	2.54	2.26	1.38	1.45	2.62	1.81
	VQ	5.00	4.96	4.78	4.34	4.36	4.54	4.06	4.04	4.00	4.46	4.65	2.92	4.56	4.28
	IF	4.54	4.20	4.50	4.38	4.04	2.08	3.52	1.80	1.54	1.46	1.29	1.51	1.32	1.28
	KP	4.66	4.26	4.48	4.20	3.90	1.88	3.76	1.90	1.38	1.37	1.38	1.45	1.44	1.30
	Avg	4.56	4.41	4.46	4.06	3.96	3.09	3.36	2.42	2.37	2.39	2.17	1.83	2.49	2.17
Humidity	VC	4.50	4.40	4.40	3.66	3.82	4.40	2.68	2.32	2.28	1.94	1.76	1.62	2.86	1.40
	VQ	4.94	4.90	4.94	4.62	4.58	4.94	4.42	4.32	4.14	4.50	4.56	3.52	4.62	4.28
	IF	3.92	3.52	4.74	4.56	3.28	1.52	3.36	2.22	1.34	1.54	1.88	1.90	1.72	1.36
	KP	4.26	3.76	4.78	4.22	3.44	1.60	3.36	2.16	1.44	1.64	2.20	2.06	1.90	1.40
	Avg	4.41	4.15	4.72	4.20	3.78	3.12	3.46	2.76	2.30	2.41	2.60	2.28	2.78	2.11
Acidity	VC	4.46	4.36	3.92	3.42	3.94	4.74	2.74	2.60	3.14	1.88	1.34	1.38	2.74	1.60
	VQ	5.00	4.76	4.94	4.75	4.76	4.88	4.28	4.40	4.28	4.68	4.70	3.32	4.40	4.26
	IF	3.82	3.58	4.38	4.02	3.50	1.20	2.36	1.40	1.10	1.08	1.12	1.22	1.18	1.12
	KP	3.70	3.44	4.06	3.91	3.68	1.20	2.34	1.40	1.06	1.08	1.14	1.26	1.14	1.04
	Avg	4.25	4.04	4.33	4.03	3.97	3.01	2.93	2.45	2.40	2.18	2.08	1.80	2.37	2.01
Light	VC	3.70	4.40	4.24	3.34	3.82	4.64	2.84	2.36	2.44	1.88	1.45	1.43	2.66	1.54
	VQ	4.78	4.92	4.96	4.51	4.68	4.84	4.46	4.26	4.26	4.48	4.71	2.98	4.50	4.20
	IF	4.40	2.88	4.44	3.77	3.74	1.86	3.60	2.64	1.98	2.31	2.22	2.11	1.62	1.41
	KP	4.64	3.50	4.58	4.46	4.12	2.22	3.84	3.00	2.20	2.67	2.67	2.28	2.06	1.83
	Avg	4.38	3.93	4.56	4.02	4.09	3.39	3.69	3.07	2.72	2.83	2.77	2.20	2.71	2.25
Break	VC	4.80	4.90	4.64	4.14	4.74	4.88	4.00	2.98	2.98	1.80	1.36	1.46	2.36	1.40
	VQ	4.92	4.78	4.94	4.82	4.48	4.72	4.12	4.06	4.54	4.46	4.64	3.28	4.50	4.14
	IF	4.06	4.34	4.58	4.66	4.56	2.36	3.10	2.18	1.40	1.10	1.36	1.62	1.08	1.22
	KP	3.84	4.14	4.38	4.61	4.36	2.06	2.72	1.92	1.24	1.02	1.30	1.46	1.10	1.14
	Avg	4.41	4.54	4.64	4.56	4.54	3.51	3.49	2.79	2.54	2.10	2.17	2.00	2.26	1.98
Inflate	VC	4.53	4.88	4.63	3.78	4.20	4.54	3.00	2.53	2.38	1.94	1.59	1.31	2.58	1.56
	VQ	4.94	4.98	4.65	4.58	4.46	4.92	4.46	4.12	3.98	4.47	4.57	3.20	4.70	4.15
	IF	4.22	3.56	3.82	4.56	3.96	1.48	3.34	3.14	2.12	2.67	2.33	2.08	1.64	1.65
	KP	4.31	3.36	3.51	3.88	3.70	1.46	3.06	2.94	1.78	2.37	2.37	1.74	1.5	1.60
	Avg	4.50	4.20	4.15	4.20	4.08	3.10	3.47	3.18	2.57	2.86	2.71	2.08	2.61	2.24
Squeeze	VC	4.44	4.80	4.56	3.52	4.14	4.68	3.12	2.46	2.92	2.26	1.53	1.48	2.36	1.79
	VQ	4.94	4.94	4.76	4.77	4.34	4.82	3.88	4.12	4.24	4.62	4.51	3.22	4.24	4.27
	IF	2.86	2.54	3.78	2.59	3.38	1.22	2.56	1.90	1.42	1.36	1.64	1.48	1.24	1.46
	KP	2.74	2.48	3.82	3.62	3.04	1.22	2.28	1.70	1.32	1.34	1.30	1.30	1.20	1.38
	Avg	3.75	3.69	4.23	3.63	3.73	2.99	2.96	2.55	2.48	2.39	2.25	1.87	2.26	2.22
Twist	VC	4.52	4.52	4.68	4.24	4.3	4.52	2.56	2.22	2.62	2.02	1.63	1.43	1.84	1.66
	VQ	4.90	5.00	4.86	4.52	4.32	4.98	4.74	4.24	4.02	4.45	4.55	3.31	4.12	4.25
	IF	3.86	3.72	4.22	3.99	4.14	1.78	3.00	2.38	1.76	1.61	1.59	1.82	1.12	1.46
	KP	3.80	3.94	3.80	3.77	3.88	1.78	2.80	2.28	1.62	1.65	1.61	1.71	1.10	1.46
	Avg	4.27	4.30	4.39	4.13	4.16	3.27	3.28	2.78	2.51	2.43	2.35	2.07	2.05	2.21
Stretch	VC	4.36	4.34	4.26	3.80	3.98	4.20	3.22	2.38	2.36	2.07	1.90	1.54	2.10	1.51
	VQ	5.00	4.98	4.90	4.72	4.54	4.72	4.52	3.98	4.14	4.54	4.59	3.10	4.10	3.79
	IF	4.44	3.84	4.06	3.96	3.96	2.00	3.44	2.60	2.18	2.33	2.55	2.06	1.08	1.04
	KP	4.52	3.76	4.10	4.18	4.10	2.12	3.48	2.50	2.10	2.48	2.71	2.04	1.08	1.21
	Avg	4.58	4.23	4.33	4.19	4.15	3.26	3.67	2.87	2.70	2.85	2.94	2.19	2.09	1.89
Causal	VC	4.26	4.46	4.56	4.18	4.22	3.96	3.20	2.68	2.20	3.54	2.10	2.08	2.50	1.86
	VQ	4.88	4.84	4.98	4.76	4.84	4.76	4.16	4.66	3.84	4.88	4.71	3.66	4.28	4.12
	IF	4.74	4.58	4.78	4.35	4.04	2.50	3.50	2.54	2.18	1.56	1.88	2.24	1.74	1.80
	KP	4.68	4.56	4.84	4.13	3.96	2.70	3.38	2.52	2.10	1.56	1.90	2.20	1.72	1.96
	Avg	4.64	4.61	4.79	4.36	4.27	3.48	3.56	3.10	2.58	2.89	2.65	2.55	2.56	2.44
Overall	Avg	4.36	4.22	4.45	4.12	4.07	3.21	3.35	2.76	2.52	2.51	2.46	2.09	2.44	2.14

consumption associated with training such large models may also limit the accessibility and sustainability of this approach in resource-constrained environments. Future work will need to address these scalability concerns, possibly through model distillation or optimization techniques.

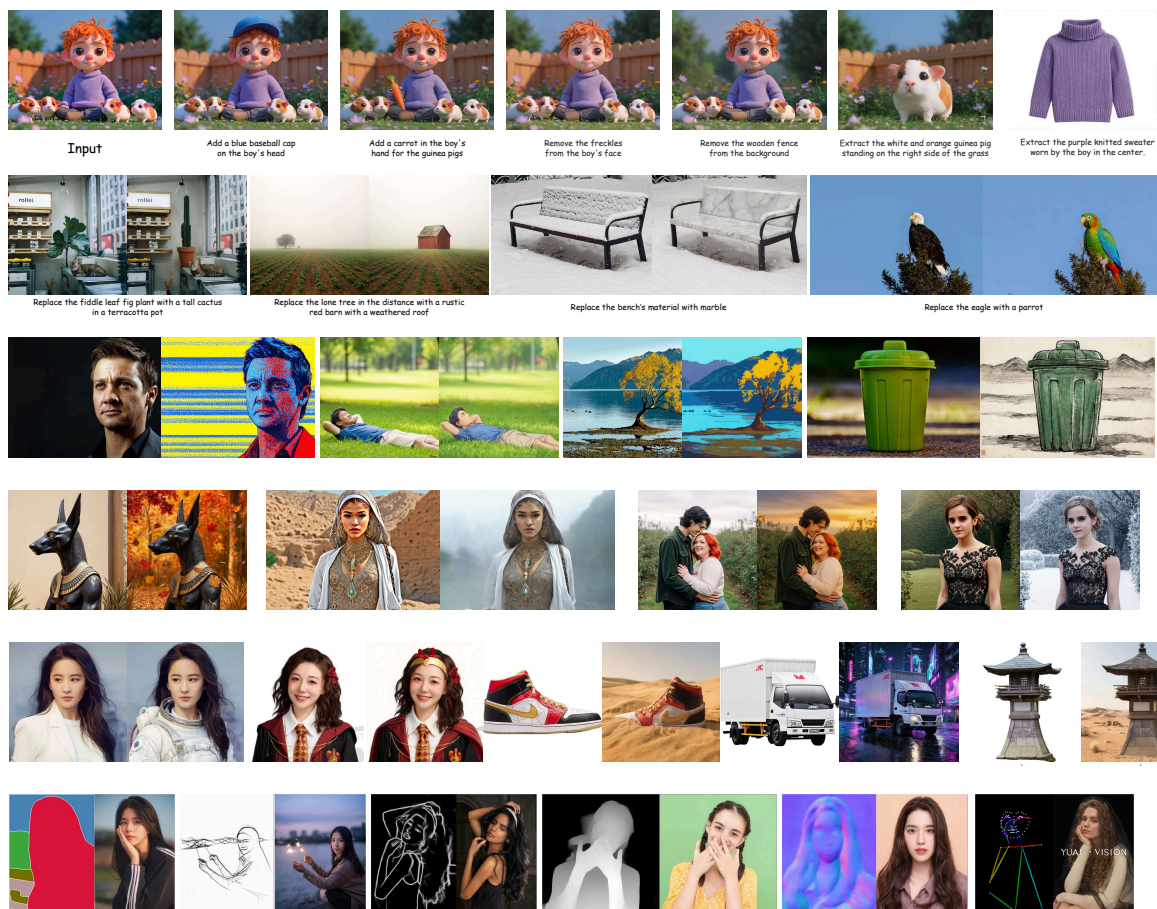


Figure 13: **More results on single image editing.** From top to bottom: (1) *Add/Remove/Extract*: adding objects, removing elements, and extracting subjects; (2) *Replace*: substituting objects or materials while preserving context; (3) *Style Transfer*: transforming image appearance into different artistic styles; (4) *Background*: modifying or replacing image backgrounds; (5) *Subject-Driven Generation*: generating new images conditioned on reference subjects; (6) *Controllable Generation*: generating images with spatial or structural control signals.

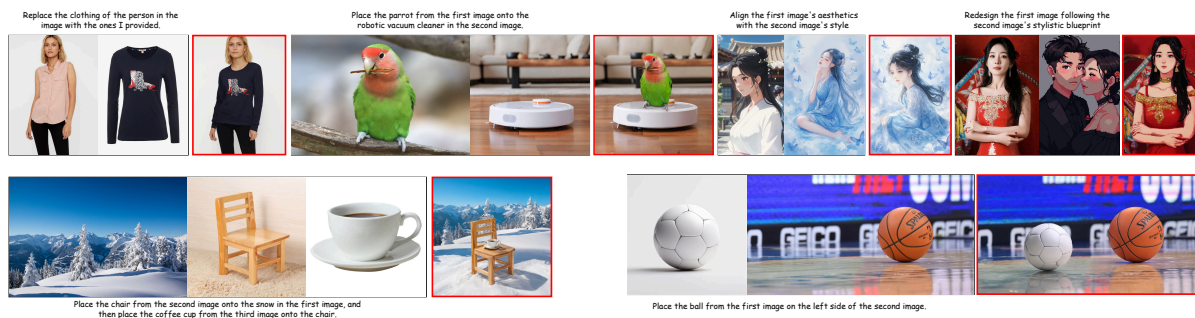


Figure 14: **More results on multi-element composition.** Our model can compose multiple reference subjects into a coherent scene while preserving the identity of each element.

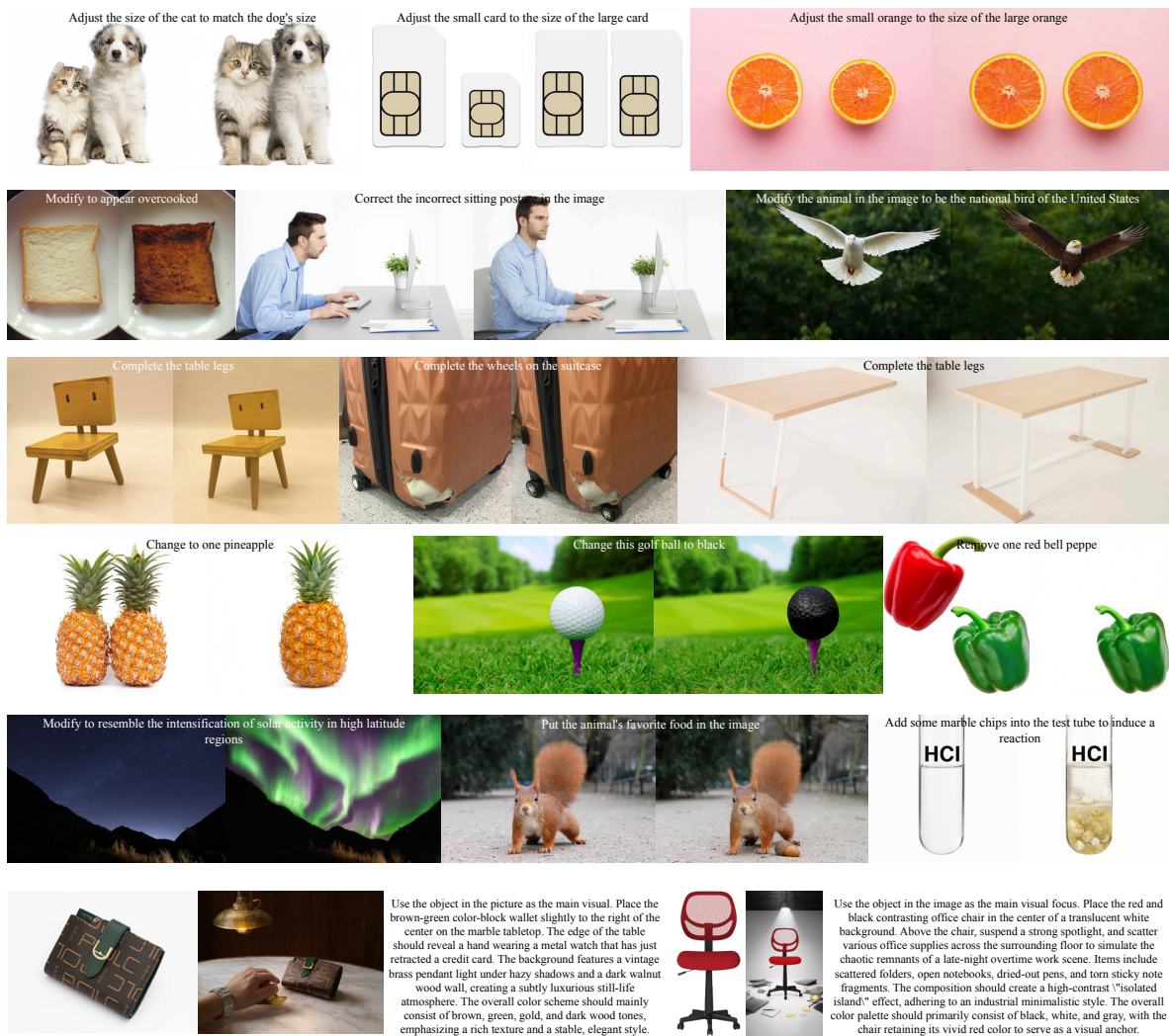


Figure 15: **More results on intelligent image editing.** These examples require complex world knowledge such as biological transformations, geographical understanding, and cultural context to perform accurate editing.

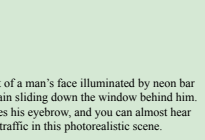
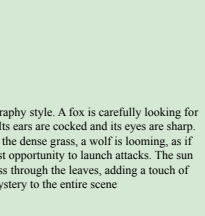
Input	Output Image	Output CoT
<p>Actions taken by animals in the image to beg for food</p>		<p>&lt;think&gt;The original instruction asks for an edit based on a description of animals begging for food. Upon analyzing the reference image, I see two small birds with pink feathers and yellow beaks inside a nest. The birds are already in a posture that suggests they are looking up, which aligns with the concept of begging. To fulfill the user's request, I need to interpret the abstract action of begging and translate it into concrete visual changes for the birds. The most effective way to show a bird begging is to change its pose from looking up to actively reaching up with its beak. I will reason that the birds should be depicted with their beaks wide open, as if they are calling out or pleading for food. This change requires modifying the shape of their beaks and the surrounding feathers to accommodate the open-mouthed pose. I must also ensure that the rest of the image, including the nest and the background, remains unchanged to maintain the focus on the birds' behavior. The resulting instruction should clearly describe these specific modifications to the birds' heads and beaks while preserving the overall scene.&lt;/think&gt;</p>
<p>The organism in the image makes changes to blend into the environment</p>		<p>&lt;think&gt;The chameleon's body adapts a muted, sandy palette, replacing its vibrant greens with earthy browns and tans. Its skin texture appears more granular and less smooth, aiding in concealment among dry leaves. The distinctive striped pattern is reinterpreted with subdued, mud-like shades, and the prominent spikes along its back are camouflaged with patches of lichen. The eye blends into the head, lacking its former intensity, while its limbs and body adopt a slightly twisted posture, mimicking the irregular shapes of branches.&lt;/think&gt;</p>
<p>Adjust the size of the cat to match the dog's size</p>		<p>&lt;think&gt;The user wants to adjust the relative size of the two animals in the reference image to create a more balanced composition. The reference image features a small, young dog standing behind a kitten, which creates a significant size disparity. The instruction asks to adjust the size of the cat to match the dog's size. This involves enlarging the kitten's head, torso, and limbs so that it no longer looks like a miniature version of the dog but rather a small cat of comparable stature. The goal is to make the two animals appear as if they are standing side-by-side of similar height against the white background, while keeping their original positions and poses intact.&lt;/think&gt;</p>
<p>A close-up portrait of a man's face illuminated by neon bars, droplets of rain sliding down the window behind him. A faint scar crosses his eyebrow, and you can almost hear distant city traffic in this photorealistic scene.</p>		<p>&lt;think&gt;First, I'll diagnose the user's input. The request is for a 'photorealistic scene' of a man, which means the primary goal is to achieve a high degree of realism and emotional depth. The core elements are the man, the neon lights, the rain, and the urban atmosphere. The thought process must therefore focus on translating these abstract concepts into concrete, sensory details that a camera would capture. The first step is to establish the composition and subject. The prompt specifies a 'close-up portrait', so I will frame the shot to make the man's face the undeniable focal point. To move beyond a generic 'man', I'll define his specific physical characteristics, such as ethnicity and hair, to give him a distinct identity. The pose and gaze are also critical; having him look directly at the viewer creates an immediate connection and a sense of intimacy. Next, I'll build the environment and its interaction with the subject. The 'window with rain' is a key element. To make it feel real, I need to describe its physical properties. Specifying the shape and behavior of the 'droplets' and adding 'reflections' to the glass surface is essential for creating a believable sense of depth and texture between the viewer and the subject. The lighting is the most crucial element for creating mood. The prompt mentions 'neon bars', which are the primary light source. To make this effect tangible, I must first define the specific colors of the neon lights. More importantly, I need to describe 'how' this light interacts with the scene. I'll detail the colored light falling on the man's face, creating strong highlights and shadows. This high-contrast lighting scheme is what will sculpt his features and enhance the dramatic, moody atmosphere. Finally, I'll address the background and the overall photographic style. The prompt's mention of 'distant city traffic' and 'almost hear sounds' is a call for a specific photographic technique. To create a sense of a bustling, out-of-focus city at night without showing it explicitly, I'll use a 'shallow depth of field'. This blurs the background into abstract shapes and 'bokeh' lights, which accomplishes two things: it creates a beautiful visual effect and reinforces the idea of a distant, unseen world. Unifying all these elements under a 'photorealistic' style ensures the final output aims for sharp focus, natural textures, and authentic lighting.&lt;/think&gt;</p>
<p>The style is photography style. A fox is carefully looking for food in the forest. Its ears are cocked and its eyes are sharp. In the distance, in the dense grass, a wolf is looming, as if waiting for the best opportunity to launch attacks. The sun shines on the grass through the leaves, adding a touch of mystery to the entire scene</p>		<p>&lt;think&gt;Based on the user's request for a photorealistic wildlife scene, my thought process prioritizes composition, subject detail, and atmospheric lighting to transform the simple description into a dramatic and believable moment. First, I'll establish the composition and narrative focus. The prompt mentions a fox 'looking for food' and a wolf 'looming'. To visually translate this power dynamic, I'll position the fox as the primary subject, placing it in the foreground and making it the central point of action. This immediately establishes it as the protagonist in this confrontation. The wolf will be placed in the background, partially obscured by the environment, to visually represent its role as a lurking threat. This creates a clear visual hierarchy and a story. Next, I'll flesh out the subjects with specific details to enhance realism and character. The genre 'fox' and 'wolf' need to be given distinct features. I'll define the fox's posture and action more precisely, describing how it lowers its head to sniff the ground, which makes the 'looking for food' action more concrete. I'll also specify its fur color and markings to give it a unique identity. For the wolf, describing it as a 'silhouette' is a deliberate choice to heighten its menace and make it feel more like a shadowy, mysterious threat rather than a detailed creature. Adding a 'glint in its eye' is a small but crucial detail to inject a sense of life and focus. Then, I'll build out the environment and lighting to create the requested 'mystery'. The 'dense grass' needs more texture to feel real, so I'll add elements like 'dry leaves' and 'thin stalks' to create a more complex and natural setting. The 'sun shines on the grass' is a great starting point, but to achieve the 'mystery', I need to define its quality. I'll specify a 'warm, golden light' and describe how it filters through an overhead canopy, creating a 'dappled effect' of light and shadow. This not only adds visual interest but also enhances the sense of a hidden, untamed wilderness. Finally, I'll unify all these elements under a consistent photographic style. To emphasize the fox as the focal point and create a more intimate and dramatic perspective, I'll incorporate a 'shallow depth of field'. This photographic technique renders the background, including the wolf, in a soft blur, which serves two purposes: it isolates the main subject and reinforces the fox as a distant, secondary element. This choice of lens language elevates the scene from a simple description to a professional, cinematic photograph.&lt;/think&gt;</p>

Figure 16: **Chain-of-thought enhanced generation and editing.** For each example, we show the generated image along with the corresponding thinking process enclosed in <think> tokens. The model first reasons about the required visual transformation, then generates the output image accordingly.